https://doi.org/10.5194/egusphere-2022-1423
Preprint. Discussion started: 31 January 2023

Process-oriented models of autumn leaf phenology: ways to sound calibration and implications of uncertain projections

Michael Meier, Christof Bigler
Forest Ecology, Department of Environmental Systems Science, ETH Zurich, Zurich, Switzerland

Correspondence to: Michael Meier (michael.meier@usys.ethz.ch)

Abstract. Autumn leaf phenology marks the end of the growing season, during which trees assimilate atmospheric CO_2. Since autumn leaf phenology responds to climatic conditions, climate change affects the length of the growing season. Thus, autumn leaf phenology is often modelled to assess possible climate change effects on future CO_2 mitigating capacities and species compositions of forests. Projected trends have been mainly discussed with regards to model performance and climate change scenarios. However, there has been no systematic and thorough evaluation of how performance and projections are affected by the calibration approach. Here, we analyzed >2.3 million performances and 39 million projections across 21 models, 5 optimization algorithms, ≥7 sampling procedures, and 26 climate model chains from two representative concentration pathways. Calibration and validation were based on >45 000 observations for beech, oak, and larch from 500 Central European sites each.

Phenology models had the largest influence on model performance. The best performing models were (1) driven by daily temperature, day length, and partly by seasonal temperature or spring leaf phenology and (2) calibrated with the Generalized Simulated Annealing algorithm (3) based on systematically balanced or stratified samples. Assuming an advancing spring phenology, projected autumn phenology shifts between -13 and +20 days by 2080–2099, resulting in a lengthening of the growing season by 7–40 days. Climate scenarios and sites explained more than 80% of the variance in these shifts and thus had eight to 22 times the influence of phenology models. Warmer climate scenarios and better performing models predominantly extended the growing season more than cooler scenarios and poorer models.

Our results justify inferences from comparisons of process-oriented phenology models to phenology-driving processes and we advocate species-specific models for such analyses and subsequent projections. For sound calibration, we recommend a combination of cross-validations and independent tests, using randomly selected sites from stratified bins based on mean annual temperature and average autumn phenology, respectively. Poor performance and little influence of phenology models on autumn phenology projections suggest that the models are overlooking relevant drivers. While the uncertain projections indicate an extension of the growing season, further studies are needed to develop models that adequately consider the relevant processes for autumn phenology.

Key words. Climate change, deciduous trees, leaf senescence, optimization algorithms, sampling procedures, site-specific calibration, species-specific calibration, tree phenology.

https://doi.org/10.5194/egusphere-2022-1423
Preprint. Discussion started: 31 January 2023

1 Introduction

Leaf phenology of deciduous trees describes the recurrent annual cycle of leaf development from bud set to leaf fall (Lieth, 1974). In temperate and boreal regions, spring and autumn leaf phenology divide this cycle into a photosynthetically active and inactive period, hence forth referred to as the growing and dormant season (Lang et al., 1987; Maurya and Bhalerao, 2017). The response of leaf phenology to climate change affects the length of the growing season and thus the amount of atmospheric CO_2 taken up by trees (e.g. Richardson et al., 2013; Keenan et al., 2014; Xie et al., 2021), as well as species distribution and species composition (e.g. Chuine and Beaubien, 2001; Chuine, 2010; Keenan, 2015). While several studies found spring phenology to advance due to climate warming (e.g. Fu et al., 2014a; Meier et al., 2021), findings regarding autumn phenology are more ambiguous (Piao et al., 2019; Menzel et al., 2020) but tend to indicate a backward shift (e.g. Bigler and Vitasse, 2021; Meier et al., 2021).

Various models have been used to study leaf phenology and provide projections, which may be grouped in correlative and process-oriented models (Chuine et al., 2013). Both types of models have served to explore possible underlying processes (e.g. Xie et al., 2015; Lang et al., 2019). The former models have often been used to analyze the effects of past climate change on leaf phenology (e.g. Asse et al., 2018; Meier et al., 2021), while the latter models have usually been applied to study the effects of projected climate change (e.g. Morin et al., 2009; Zani et al., 2020). Popular representatives of the correlative models applied in studies on leaf phenology are based on linear-mixed effects models and generalized additive models (e.g. Xie et al., 2018; Menzel et al., 2020; Meier et al., 2021; Vitasse et al., 2021), while the many different process-oriented phenology models all go back to the growing-degree day model (Chuine et al., 2013; Chuine and Régnière, 2017; Fu et al., 2020) of De Réaumur (1735).

Different process-oriented models rely on different assumptions regarding the driving processes of leaf phenology (e.g. Meier et al., 2018; Chuine et al., 1999), but their functionality is identical. Process-oriented leaf phenology models typically consist of one or more phases during which daily rates of relevant driver variables are accumulated until a corresponding threshold is reached (Chuine et al., 2013; Chuine and Régnière, 2017). The rate usually depends on daily meteorological drivers and sometimes on daylength (Chuine et al., 2013; Fu et al., 2020), while the threshold either is a constant (Chuine et al., 2013), depends on latitude (Liang and Wu, 2021) or on seasonal drivers (e.g. the timing of spring phenology with respect to autumn phenology; Keenan and Richardson, 2015).

Models of spring phenology regularly outcompete models of autumn phenology by several days when assessed by the root mean square error between observed and modelled dates (4–9 vs. 6–13 days, respectively; Basler, 2016; Liu et al., 2020). These errors have been interpreted in different ways and have multiple sources. Basler (2016) compared over 20 different models and model combinations for spring leaf phenology of trees. He concluded that inter-annual variability was underestimated in general, and that inter-site transferability of the calibrated models was not given. Liu et al. (2020) compared

https://doi.org/10.5194/egusphere-2022-1423
Preprint. Discussion started: 31 January 2023

six models of autumn leaf phenology of trees and concluded that the inter-annual variability was well represented by the models, while their representation of the inter-site variability was relatively poor.

Well-calibrated models of autumn leaf phenology are a prerequisite for sound conclusions about phenology-driving processes and for reducing uncertainties in phenological projections under distant climatic conditions. Studies of leaf phenology models generally show that certain models lead to better results and thus conclude that these models consider the relevant phenology-driving processes more accurately or add an important piece to the puzzle (Delpierre et al., 2009; Keenan and Richardson, 2015; Lang et al., 2019; Liu et al., 2019; Zani et al., 2020). Such conclusions can be assumed to be stronger if they are based on sound calibration and validation. However, so far, different calibration and validation methods have been applied (e.g. species- or site-specific calibration; Liu et al., 2019; Zani et al., 2020), which makes the comparison of study results difficult. Moreover, the uncertainty in phenology projections is related to climate projections and phenology models. While the uncertainty associated with climate projections has been extensively researched (e.g. Palmer et al., 2005; Foley, 2010; Braconnot et al., 2012), so far the uncertainty associated with process-oriented phenology models has only been described in a few notable studies: Basler (2016) compared spring phenology models calibrated per species and per site as well as calibrated per species with pooled sites, Liu et al. (2020) compared autumn phenology models with a focus on inter-site and inter-annual variability, and Liu et al. (2021) focused on sample size and observer bias in observations of spring and autumn phenology. Therefore, this uncertainty and its drivers are arguably largely unknown and thus poorly understood, which may be part of the reason for debates such as the one surrounding the Zani et al. (2020) study (Norby, 2021; Zani et al., 2021; Lu and Keenan, 2022).

When considering phenology data from different sites, one must, in principle, decide between two calibration modes, namely a calibration per site and species or a calibration over various sites with pooled data per species. While the former calibration leads to a set of parameters per species and site, the latter leads to one set of parameters per species. On the one hand, site-specific models may respond to relevant but unconsidered drivers. For example, a model based solely on temperature may provide accurately modelled data due to site-specific thresholds, even if the phenological observations at some sites are driven by additional variables such as soil water balance. On the other hand, species-specific models may be better suited for projections to new sites and changed climatic conditions, as they apply to the whole species and follow a space-for-time approach.

Independent of the calibration mode, various optimization algorithms have been used for the calibration of the model parameters. The resulting parameters are often intercorrelated (e.g. the base temperature for the growing degree days function and the corresponding threshold value to reach) and the parameter space may have various local optima (Chuine and Régnière, 2017). To calibrate phenology models, different optimization algorithms have been applied to locate the global optimum, such as simulated annealing, particle swarm optimization, or Bayesian optimization methods (e.g. Chuine et al., 1998; Liu et al., 2020; Zhao et al., 2021). Simulated annealing and its derivatives seem to be most used in the calibration of process-oriented models of tree leaf phenology (e.g. Chuine et al., 1998; Basler, 2016; Liu et al., 2019; Zani et al., 2020). However, a systematic

https://doi.org/10.5194/egusphere-2022-1423
Preprint. Discussion started: 31 January 2023

comparison of these different optimization algorithms regarding their influence on model performance and projections has been missing so far.

Previous studies on process-oriented phenology models have generally considered all sites in a given dataset and provided little information on the sampling procedure used to assign observations to the calibration or validation sample. Observations and sites may be sampled according to different procedures, such as random, stratified, or systematic sampling (Taherdoost, 2016). In contrast to random sampling, systematic and stratified sampling require a basis to which the systematic or stratification refers to. For example, when assigning observations based on year, observations from every i^{th} year or one randomly selected observation from each of the i bins with equal time spans may be selected in systematic or stratified sampling, respectively. Studies on phenology models have usually considered all sites of the underlying dataset and declared the size of calibration and validation samples or the number of groups (k) in a k-fold cross-validation (e.g. Delpierre et al., 2009; Basler, 2016; Meier et al., 2018). However, the applied sampling procedure has not always been specified, but there are notable exceptions, such as Liu et al. (2019) for random sampling, Chuine et al. (1998) for systematic sampling, and Lang et al. (2019) for leave-one out cross-validation. Moreover, the effects of the sampling procedure on the performance and projections of process-oriented phenology models have not been studied yet.

Sample size in terms of the number of observations per site and the number of sites may influence the quality of phenology models as well. Studies on phenology models have usually selected sites with at least 10 or 20 observations per site, independent of the calibration mode (e.g. Delpierre et al., 2009; Keenan and Richardson, 2015; Lang et al., 2019). In contrast, we found a wide range in the number of sites that have been considered in studies with species-specific models, namely 8 to >800 sites (e.g. Liu et al., 2019; Liu et al., 2020). In site-specific calibration, the number of sites may be neglected as the site-specific models cannot be applied to other sites. However, the number of observations per site is crucial, as small samples may lead to overfitted models due to the bias-variance trade-off (James et al., 2017, Ch. 2.2.2), i.e. the trade-off between minimizing the prediction error in the validation sample versus the variance of the estimated parameters in the calibrated models. To our knowledge, no study to date has examined possible overfitting in site-specific phenology models. In addition, in species-specific calibration, the number of sites could influence the degree to which the population is represented by the species-specific models. While such reasoning appears intuitively right, we are unaware of any study that has systematically researched the correlation between the number of sites and the degree of representativeness.

Phenology models are typically calibrated, their performance is estimated, and some studies project leaf phenology under distant climatic conditions. The performance of phenology models has often been estimated with the root mean square error that is calculated from modelled and observed data (e.g. Delpierre et al., 2009; Lang et al., 2019) and has been generally used for model comparison (e.g. Basler, 2016; Liu et al., 2020) and model selection (e.g. Liu et al., 2019; Zani et al., 2020). When phenology has been subsequently projected under distant climatic conditions, projections may have been compared between models (Zani et al., 2020), but no correlation with model performance has been established yet.

With this study, we take a first step towards closing the gap of unknown uncertainties associated with process-oriented models of autumn tree leaf phenology, which has been left open by current research so far. We focused on uncertainties related to

https://doi.org/10.5194/egusphere-2022-1423
Preprint. Discussion started: 31 January 2023

phenology models, optimization algorithms, sampling procedures, and sample sizes, evaluating their effects on model performance and model projection separately in site- and species-specific calibration mode. To this end, we conducted an extensive computer experiment with 21 autumn phenology models from the literature, 5 optimization algorithms, each run with 2 different settings, and various samples based on random, structured, and stratified sampling procedures and on different sample sizes. We analyzed the performance of >2.3 million combinations of model, algorithm, sample, and calibration mode based on observations for beech, pedunculate oak, and larch from Central Europe for the years 1948–2015 (500 sites per species; PEP725; Templ et al., 2018). Further, we analyzed 39 million projections to the year 2099 according to these combinations under 26 different climate model chains, which were split between 2 different representative concentration pathways (CORDEX EUR-11; RCP 4.5 and RCP 8.5; Riahi et al., 2011; Thomson et al., 2011; Jacob et al., 2014). We addressed the following research questions:

I. What is the effect of the phenology model and calibration approach (i.e. calibration mode, optimization algorithm, and calibration sample) on model performance and projections?
II. What is the effect of sample size on the degree to which models are overfitted or represent the entire population?
III. Do better performing models lead to more accurate predictions?

2 Data and methods

2.1 Data

2.1.1 Phenological observations

We ran our computer experiment with leaf phenology observations from Central Europe for common beech (*Fagus sylvatica* L.), pedunculate oak (*Quercus robur* L.), and European larch (*Larix decidua* MILL.). All phenological data were derived from the PEP725 project database (http://www.pep725.eu/; accessed on April 13, 2022). The PEP725 dataset mainly comprises data from 1948–2015 that were predominantly collected in Austria, Belgium, Czech Republic, Germany, the Netherlands, Switzerland, and the United Kingdom (Templ et al., 2018). We only considered site-years for which the phenological data were in the proper order (e.g. the date for leaf coloration was before the date for leaf fall) and the period between spring and autumn phenology was at least 30 days. After corresponding correction for the site-years, we only considered sites with at least 20 years for which both spring and autumn phenology data were available. We randomly selected 500 of these sites per species. Each of these sites comprised 20–65 (beech), 20–64 (oak), or 20–30 (larch) site-years, all of which included a spring and autumn phenology datum. This added up to 17 211 site-years for beech, 16 954 site-years for oak, and 11 602 site-years for larch. Spring phenology corresponded to leaf unfolding (BBCH11) for beech and oak and leaf separation (BBCH10) for larch, while autumn phenology for all three species was represented by leaf coloration (BBCH94; Hack et al., 1992; Meier, 2001).

https://doi.org/10.5194/egusphere-2022-1423
Preprint. Discussion started: 31 January 2023

The 500 selected sites per species differed in location as well as in leaf phenology and climatic conditions. Most sites were from Germany but also from other countries such as Slovakia or Norway (Fig. 1). Autumn phenology averaged over selected site-years per site ranged from day of year 254–308 (beech), 265–309 (oak), and 261–314 (larch). Corresponding average mean annual temperatures ranged from 0.6–11.0 °C (beech), 6.3–11.0 °C (oak), and 4.1–11.0 °C (larch) and annual precipitation ranged from 470–1272 mm (beech), 456–1232 mm (oak), and 487–1229 mm (larch; Fig. 1).

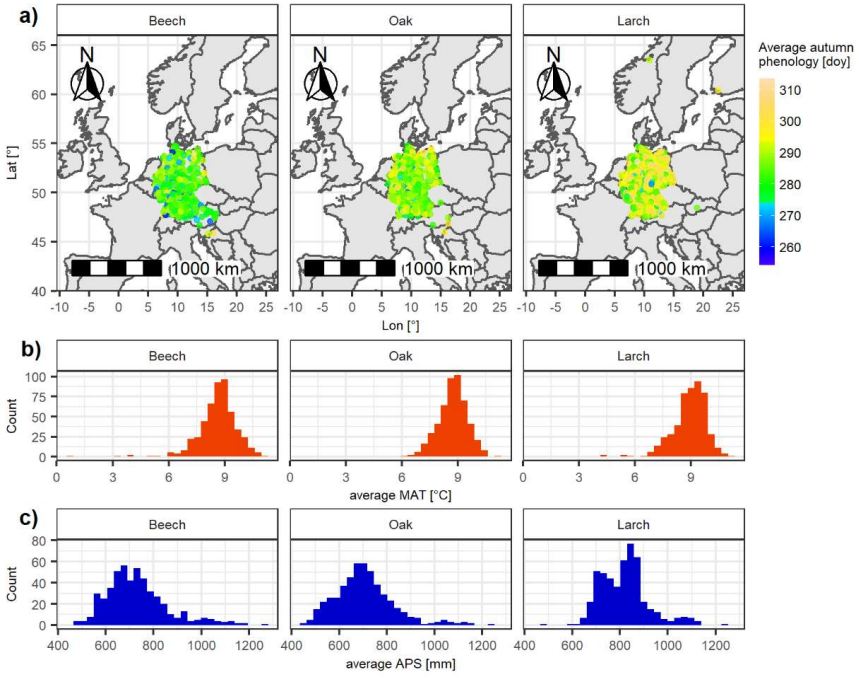

Figure 1: Sites of considered leaf phenology data with respective average climatic conditions for beech, oak, and larch. (a) The location of each site is marked with a dot, the color of which indicates the average day of year of autumn phenology. (b) and (c) show the distribution of average mean annual temperature (MAT; [°C]) and average annual precipitation sum (APS; [mm]) per site.

2.1.2 Model drivers

The daily and seasonal drivers of the phenology models were derived and calculated from interpolated daily weather data as well as data of different time scales of short- and longwave radiation, atmospheric CO_2 concentration, leaf area indices, and soil moisture. Daily drivers are daily minimum air temperature which is mostly combined with day length. Some models further consider seasonal drivers, which we derived from daily mean and maximum air temperature, precipitation, soil moisture, net and downwelling shortwave radiation, and net longwave radiation, from monthly leaf area indices, from monthly

https://doi.org/10.5194/egusphere-2022-1423
Preprint. Discussion started: 31 January 2023

or yearly atmospheric CO_2 concentration data, as well as from site-specific plant-available water capacity data. We calculated day length according to latitude and day of year (Supplement S3: Eq. S1; Brock, 1981). The other daily variables were derived from two NASA global land data assimilation system datasets on a 0.25°× 0.25° grid (~25 km; GLDAS-2.0 and GLDAS-2.1 for the years 1948–2000 and 2001–2015, respectively; Rodell et al., 2004; Beaudoing and Rodell, 2019, 2020) for the past and from the CMIP5-based CORDEX-EUR-11 datasets on a rotated 0.11° × 0.11° grid (~12.5 km; for the years 2006–2099; Riahi et al., 2011; Thomson et al., 2011; Jacob et al., 2014) for two representative concentration pathways (RCP). After examining the climate projection data (Supplement S1: Sect. 2), we remained with 16 and 10 climate model chains (CMC) for the RCP 4.5 and 8.5, respectively. Atmospheric CO_2 concentrations were derived from the historical CMIP6 and observational Mauna Loa datasets for the years 1948–2014 and for 2015, respectively (monthly data; Meinshausen et al., 2017; Thoning et al., 2021) for the past and from the CMIP5 datasets for the years 2006–2099 (yearly data; Meinshausen et al., 2011) for the climate projections, matching the RCP 4.5 and RCP 8.5 scenarios (Smith and Wigley, 2006; Clarke et al., 2007; Wise et al., 2009; Riahi et al., 2007). Leaf area indices were derived from the GIMMS-LAI3g dataset on a 0.25° × 0.25° grid, averaged over the years 1981–2015 (Zhu et al., 2013; Mao and Yan, 2019). The plant-available water capacity per site was derived directly or estimated according to soil composition (i.e. volumetric silt, sand, and clay contents) from corresponding ISRIC SoilGrids250m datasets on a 250 m × 250 m grid (versions 2017-03 or 2.0 for water content or soil composition, respectively; Hengl et al., 2017). More detailed information about the applied driver data and driver calculation is given in Supplement S1 and S3, respectively.

2.2 Phenology models

We based our analysis on 21 process-oriented models of autumn phenology, which differ in their underlying functions and/or the daily and seasonal drivers they consider (Table 1; Meier, 2022). In all models, the projected date for autumn phenology corresponds to the first day of the year, for which an accumulated daily senescence rate (R_S) exceeds a corresponding threshold value. The daily senescence rate responds to daily minimum temperature and, except for the CDD model (see Table 1 and Supplement S2), to day length. While the senescence rate increases with colder temperatures, it may increase or decrease with shorter days, depending on the response function. Thus, with colder temperatures, the rate follows either a monotonically increasing response curve (with $R_S \geq 0$) or a sigmoidal response curve (with $0 \leq R_S \leq 1$), with the monotonous increase amplified or weakened with shorter days, depending on the model (Dufrêne et al., 2005; Delpierre et al., 2009; Lang et al., 2019). The threshold value for the accumulated rate is either a constant or depends linearly on one or two seasonal drivers. Accumulation of the daily rate starts on the first day after the 173rd day of the year (summer solstice) or after the 200th day of year, for which minimum temperature and/or day length fall below corresponding thresholds. The models have between 2 and 7 free parameters, which are jointly fitted during calibration.

https://doi.org/10.5194/egusphere-2022-1423
Preprint. Discussion started: 31 January 2023

Table 1. Compared process-oriented models of autumn phenology grouped according to their response curve for the daily senescence rate and their corresponding threshold function.

Response curve (threshold function)	Model	Daily drivers	Seasonal drivers	Number of free parameters	Source
MInc (Co)	CDD	T	-	2	Du05
MInc– (Co)	DM1	T, L	-	5	De09
	$DM1_{Za20}$			3	Za20
MInc– (Li)	SIAM	T, L	a.dSP	4	Ke15
	TDM1		T_{LS}	6	Li19
	PDM1		LPI_{LS}	6	Li19
	TPDM1		T_{LS}, LPI_{LS}	7	Li19
MInc+ (Co)	DM2	T, L	-	5	De09
	$DM2_{Za20}$			3	Za20
MInc+ (Li)	TDM2	T, L	T_{LS}	6	Li19
	PDM2		LPI_{LS}	6	Li19
	TPDM2		T_{LS}, LPI_{LS}	7	Li19
Sig (Co)	TPMt	T, L	-	4	La19
	TPMp			4	La19
Sig (Li)	$SIAM_{Za20}$	T, L	a.dSP	5	Za20
	TDM_{Za20}		T_{GS}	5	Za20
	PDM_{Za20}		LPI_{Za20}	5	Za20
	$TPDM_{Za20}$		T_{GS}, LPI_{Za20}	6	Za20
	PIA_{GSI}		a.GSI	5	Za20
	PIA^{+}		$a.A_{net}$	5	Za20
	PIA^{-}		$a.A_{net-w}$	5	Za20

Note: Daily senescence rate responds to the daily drivers minimum temperature (T) and day length (L), following either a monotonically increasing curve (Mon) with colder temperatures, which may be weakened or amplified with shorter days (Mon– or Mon+), or a sigmoidal curve (Sig). The threshold value is either a constant (Co) or a linear function (Li) of one or two of the following seasonal drivers: site-specific anomaly of (1) spring phenology (a.dSP), (2) growing season index (a.GSI), and (3) daytime net photosynthesis accumulated during the growing season ignoring or considering water limitation constraints ($a.A_{net}$ and $a.A_{net-w}$), as well as the actual (4) leafy season or growing season mean temperature (T_{LS} and T_{GS}), (5) low precipitation index averaged over the leafy season (LPI_{LS}), or (6) growing season adapted low precipitation index (LPI_{Za20}). Further, the number of free parameters fitted during model calibration and the sources for each model are listed. (De09: Delpierre et al. (2009); Du05: Dufrêne et al. (2005); Ke15: Keenan and Richardson (2015); La19: Lang et al. (2019); Li19: Liu et al. (2019); Za20: Zani et al. (2020).) All models are explained in detail in Supplement S2).

https://doi.org/10.5194/egusphere-2022-1423
Preprint. Discussion started: 31 January 2023

2.3 Model calibration and validation

2.3.1 Calibration modes

We based our study on both a site- and species-specific calibration mode. In the site-specific mode, we derived for every calibration a species- and site-specific set of parameters (i.e. every combination of optimization algorithm and sample). In the species-specific mode, we derived for every calibration a species-specific set of parameters based on the observations from more than one site, depending on the calibration sample. Model performances were estimated with an external model validation, namely with a 5-fold cross-validation (James et al., 2017, Ch. 5.1.3) and a separate validation sample in the site- and species-specific mode, respectively.

2.3.2 Optimization algorithms

We calibrated the models with five different optimization algorithms, which can be grouped into Bayesian and non-Bayesian algorithms. The two Bayesian algorithms that we evaluated are Efficient Global Optimization algorithms based on kriging (Krige, 1951; Picheny and Ginsbourger, 2014): one is purely Bayesian (EGO), whereas the other combines Bayesian optimization with a deterministic trust-region formation (TREGO). The three non-Bayesian algorithms that we evaluated are Generalized Simulated Annealing (GenSA; Xiang et al., 1997; Xiang et al., 2013), Particle Swarm Optimization (PSO; Clerc, 2011, 2012; Marini and Walczak, 2015), and Covariance Matrix Adaptation with Evolutionary Strategies (CMA-ES; Hansen, 2006, 2016). Every Bayesian and non-Bayesian algorithm was executed in a normal and extended optimization mode, i.e. with few and many iterations/steps (norm. and extd., respectively; Supplement S4: Table S1). In addition, the parameter boundaries within which all algorithms searched for the global optimum (Supplement S2: Table S1) were scaled to range from 0 to 1. All algorithms optimized the free model parameters to obtain the smallest possible root mean square error (RMSE; Supplement S4: Eq. S1) between the observed and modelled days of year of autumn phenology. As the Bayesian algorithms cannot handle iterations that produce NA values (i.e. modelled day of year > 366), such values were set to day of year = 1 for all algorithms and before RMSE calculation.

2.3.3 Calibration and validation samples

Calibration and validation samples can be selected according to different sampling procedures with different bases (e.g. randomly or systematically based on the year of observation) and have different sizes (i.e. number of observations and/or number of sites). Here, we distinguished between the sampling procedures random, systematically continuous, systematically balanced, and stratified. Further, our populations consisted of sites that included between 20 and 65 years, which directly affected the sample size in the site-specific calibration mode. In the species-specific mode, we calibrated the models with samples that ranged from 2 to 500 sites.

In the site-specific mode, the observations for the 5-fold cross-validation were selected (1) randomly or (2) systematically (Supplement S4: Fig. S1). For the random sampling procedure, the observations were randomly assigned to one of five

https://doi.org/10.5194/egusphere-2022-1423
Preprint. Discussion started: 31 January 2023

validation bins. For the systematic sampling procedure, we ranked the observations based on the year, mean annual temperature (MAT), or autumn phenology date (AP) and created five equally sized samples containing continuous or balanced (i.e. every 5th) observations (see Supplement S4: Sect. 2.1 for further details regarding these procedures). Hence, every model was calibrated seven times for each of the 500 sites per species, namely with a randomized or a time-, phenology-, or temperature-based systematically continuous or systematically balanced cross-validation. This amounted to 2 205 000 calibration runs (i.e. 500 sites × 3 species × 21 models × 5 optimization algorithms × 2 optimization modes × 7 sample selection procedures) that consisted of 5 cross-validation runs each. Further, for the projections, every model was calibrated with all observations per site and species.

In the species-specific mode, we put aside 25% randomly selected observations per site and per species (rounded up to the next integer) for external validation samples and created various calibration samples from the remaining observations, selecting the different sites with different procedures. These calibration samples either contained the remaining observations of all 500 sites (full sample) or of (1) randomly selected, (2) systematically selected, or (3) stratified sites per species (Supplement S4: Fig. S2). The random and systematic samples contained the observations of 2, 5, 10, 20, 50, 100, or 200 sites. Randomly sampled sites were chosen either from the entire or half the population, with the latter being determined according to MAT and AP (i.e. colder average MAT or earlier or later average AP). The systematically sampled sites were selected according to a balanced procedure in which the greatest possible distance between sites ranked by average MAT or AP was chosen. (Note that the distance between the first and last site was 490, not 500 sites, allowing up to ten draws with a parallel shift of the first and last site.) The stratified samples consisted of one randomly drawn site from each of 12 MAT- or 17 AP-based bins. The chosen bin widths maximized the number of equal-sized bins so that they still contained at least one site (see Supplement S4: Sect. 2.2 for further details regarding these procedures). We drew five samples per procedure and size, except for the full sample, which we drew only once, as it contained fixed sites, namely all sites in the population. Altogether, this amounted to 139 230 calibration runs (i.e. 3 species × 21 models × 5 optimization algorithms × 2 optimization modes × (6 sample selection procedures × 7 sample sizes × 5 draws + 2 sample selection procedures × 5 draws + 1 sample selection procedure)) that differed in the size and selection procedure of the corresponding sample. Every calibration run was validated with the sample-specific and population-specific external validation sample. While the former consisted of the same sites as the calibration sample, the latter consisted of all 500 sites and hence was the same for every calibration run per species. Every calibration run was validated with the sample-specific and population-specific external validation sample, hence forward referred to as "validation within sample" and "validation within population". While the former consisted of the same sites as the calibration sample, the latter consisted of all 500 sites and hence was the same for every calibration run per species.

2.4 Model projections

We projected autumn phenology to the years 2080–2099 for every combination of phenology model, calibration mode, optimization algorithm, and calibration sample that converged without producing NA values, assuming a linear trend for spring phenology. While non-converging runs did not produce calibrated model parameters, we further excluded the converging runs

https://doi.org/10.5194/egusphere-2022-1423
Preprint. Discussion started: 31 January 2023

that resulted in NA values in either the calibration or validation. In addition, we excluded combinations where projected leaf senescence occurred before the 173rd or 200th day of the year (i.e. the earliest possible model-specific day of senescence rate accumulation). Thus, we received 41 901 704 site-specific time series for the years 2080–2099 of leaf senescence projected with site-specific models. These time series differed in climate projection scenario (i.e. per combination of representative concentration pathway and climate model chain), phenology model, optimization algorithm, and calibration sample. Species-specific models led to projections for all 500 sites per species (i.e. the entire populations) and thus to 1 574 378 000 time series for the years 2080–2099 that differed in climate projection scenario, model, algorithm, and calibration sample. For site- and species-specific models, we projected the spring phenology relevant for the seasonal drivers assuming a linear trend of -2 days per decade (Piao et al., 2019; Menzel et al., 2020; Meier et al., 2021). This trend was applied from the year after the last observation (ranging from 1969 to 2015, depending on site and species) and based on the respective site average over the last 10 observations per species.

2.5 Proxies and statistics

2.5.1 Sample size proxies

We approximated the effect of sample size (1) on the bias-variance trade-off and (2) on the degree to which models represent the entire population with the respective size proxies (1) number of observations per parameter and (2) site ratio. The effect of sample size on the bias-variance trade-off may depend on the number of observations in the calibration sample (N) *relative to* the number of free parameters (q) in the phenology model. In other words, a sample of, say, 50 observations may lead to a better calibration of the CDD model (2 free parameters) compared to the TPDM1 model (7 free parameters). In the site-specific calibration, we calculated for each site and model the ratio N:q with N being 80% of the total number of observations per site to account for the 5-fold cross-validation. Assuming the 50 observations in the example above are the basis for the 5-fold cross-validation, N becomes 40, resulting in N:q = 40/2 for the CDD model and N:q = 40/7 for the TPDM1 model. With species-specific calibration, we considered the *average* number of observations per site ($\bar{N}$) and calculated for each calibration sample and model the ratio $\bar{N}$:q to separate this ratio from the site ratio explained further below. Assuming the 50 observations in the example above correspond to a calibration sample based on 2 sites, $\bar{N}$ becomes 25, resulting in $\bar{N}$:q = 25/2 for the CDD model and $\bar{N}$:q = 25/7 for the TPDM1 model. The effect of sample size on the degree to which models represent the entire population with species-specific calibration may depend on the number of sites in the calibration sample (s) *relative to* the number of sites in the entire population (S; i.e. site ratio; s:S). Thus, we derived the site ratio by dividing s by 500. Note that the combined ratios $\bar{N}$:q and s:S account for the effect of the total sample size as $(\bar{N} \times s) / (q \times S) = N / (q \times S)$.

2.5.2 Model performance

We quantified the performance of each calibrated model according to the root mean square error (RMSE; Supplement S4: Eq. S1). The RMSE was calculated for the calibration and the validation samples (i.e. internal and external RMSE, respectively)

https://doi.org/10.5194/egusphere-2022-1423
Preprint. Discussion started: 31 January 2023

as well as at the sample- and population level with the species-specific calibration (i.e. validated within sample or population; external sample RMSE or external population RMSE, respectively). We derived each RMSE per sample at the site level with the site-specific calibration and at the sample level with the species-specific calibration.

To measure the effect (1) on the bias-variance trade-off and (2) on the degree to which models represent the entire population, we derived two respective RMSE ratios. Regarding the bias-variance trade-off and with the site-specific calibration, we divided the external RMSE by the internal RMSE derived from the calibration run with all observations per site and species (Cawley and Talbot, 2010, Sect. 5.2.1; James et al., 2017, Ch. 2.2.2). The numerator was expected to be larger than the denominator and increasing ratios were associated with an increasing bias, indicating overfitting. Regarding the degree to which models represent the entire population and hence with the species-specific calibration, we divided the external sample RMSE by the external population RMSE. Here, the numerator was expected to be smaller than the denominator and increasing ratios were associated with increasing representativeness.

We applied two different treatments to calibration runs that led to NA values (i.e. the threshold value was not reached by the accumulated senescence rate until day of year 366) or did not converge at all (Supplement S6: Fig. S1). On the one hand, the exclusion of such runs may bias the results regarding model performance, since a non-converging model must certainly be considered to perform worse than a converging one. Therefore, in contrast to the model calibration, we replaced the NA values with the respective observed date + 170 days (i.e. a difference that exceeds the largest modelled differences by two days) and assigned an RMSE of 170 to non-converging runs before we analyzed the model performance. On the other hand, replacing NA values with a fixed value leads to an artificial effect and affects the performance analysis, as, say, a linear dependence of the RMSE on a predictor is suddenly interrupted. Moreover, projections based on models that converged but produced NA values seem questionable, while projections based on non-converging models are impossible. Therefore, we implemented a second analysis of performance, from which we excluded the calibration runs that did not converge or contained one or more NA values in either the calibration or the validation sample. Our main results regarding model performance were based on the substituted NA values and the RMSE of 170 days for non-converging runs. However, where necessary, we have referred to the results based only on converged runs without NA values (provided in Supplement S6: Sect. 2.1.2 and 2.2.2). Furthermore, our results regarding projections and our comparisons between performance and projections are based solely on converging runs without NA values.

2.5.3 Model projections

We analyzed the autumn phenology projections according to a 100-year shift (Δ_{100}) at the site level. Δ_{100} was defined as the difference between the means of the observations for the years 1980–1999 and of the projections for the years 2080–2099. If observations for the years 1980–1999 were missing, we used the mean of the 20 last observations instead. Thus, the derived shift was linearly adjusted to correspond to 100 years.

https://doi.org/10.5194/egusphere-2022-1423
Preprint. Discussion started: 31 January 2023

2.6 Evaluation of model performance and autumn phenology projections

To answer research question I (RQ I), we calculated the mean, median, standard deviation, and skewness of the RMSE distributed across phenology models, optimization algorithms, sampling procedures, and (binned) sample size proxies. These statistics were derived separately per site- and species-specific calibration validated within sample or population, giving a first impression of the effects on model performance. Further, the distribution of the RMSE was relevant for subsequent evaluations. To answer RQ I and RQ II, we estimated the effects of phenology models, optimization algorithms, sampling procedures, and sample size proxies on model performance and, together with climate projection scenarios, on model projections with generalized additive models (GAMs; Wood, 2017) and subsequent analyses of variance (ANOVA; Chandler and Scott, 2011). We fitted the GAMs separately per site- and species-specific calibration validated (projected) within sample or population (Supplement S5: Sect. 1; Supplement S5: Eq. S1 and S2). The response variables RMSE and Δ_{100} were assumed to depend linearly on the explanatory factors phenology models, optimization algorithms, sampling procedures, and climate projection scenarios (only regarding Δ_{100}) as well as on the continuous sample size proxies as explanatory variable. Sites and species were included as smooth terms, which were set to crossed random effects such that the GAM mimicked linear mixed-effects models with random intercepts (Supplement S5: Sect. 2; Pinheiro and Bates, 2000; see the discussion for reasons and implications of our choice). The RMSE and sample size proxies were log-transformed, since they can only take positive values and followed right-skewed distributions (i.e. skew > 0; Supplement S6: Table S1–S4). Coefficients were estimated with fast restricted maximum likelihood (Wood, 2011). Thereafter, the fitted GAMs served as input for corresponding type-III ANOVA (Supplement S5: Sect. 4; Yates, 1934; Herr, 1986; Chandler and Scott, 2011), with which we estimated the influence on the RMSE and the Δ_{100}. The influence was expressed as the relative variance in RMSE or in Δ_{100} explained by (aggregated) phenology models, optimization algorithms, sampling procedures, sample size proxies, and climate projection scenarios (only regarding Δ_{100}). Regarding model projections, we drew five random samples of 10^5 projections per climate projection scenario and per Δ_{100} projected with site- and species-specific models within sample or population. Thereafter, we fitted a separate GAM and ANOVA for each of these 15 samples (see the discussion for reasons and implications of this approach).

The coefficient estimates of the GAMs expressed (relative) changes towards the corresponding reference levels of RMSE or Δ_{100}. The reference levels were based on the CDD model calibrated with the GenSA (norm.) algorithm on a randomly selected sample and, only regarding Δ_{100}, projected with the CMC 1 of the RCP 4.5. Hence, the estimates of the intercept refer to the estimated log-transformed RMSE or Δ_{100} according to these reference levels with sample size proxies of 1 (i.e. log-transformed proxies of 0). Regarding interpretation of model performance, negative coefficient estimates indicated better performance, which was reflected in smaller RMSE values. The effects of the explanatory variables were expressed as relative changes of the reference RMSE, due to the log-transformation of the latter (Supplement S5; Sect. 3). Regarding model projections, while negative coefficient estimates in combination with negative reference Δ_{100} resulted in an accelerated projected advancement of autumn phenology, they weakened a projected delay of autumn phenology or changed it to a projected advancement in combination with positive reference Δ_{100} and vice versa. In other words, negative coefficient estimates only translated into

https://doi.org/10.5194/egusphere-2022-1423
Preprint. Discussion started: 31 January 2023

earlier projected autumn phenology when the corresponding reference Δ_{100} was negative or their absolute values were larger than the (positive) reference Δ_{100} and vice versa.

To answer RQ III, we related both (1) the ranked effects on model performance to the ranked effects on model projections and (2) the performance ranks of phenology models to the ranked influence of (aggregated) explanatory variables on Δ_{100} per model. First, we ranked phenology models, optimization algorithms, and sampling procedures according to their estimated effects on log-transformed RMSE or Δ_{100}, and calculated the Kendall rank correlation (Kendall, 1938) within each group of factors (e.g. within phenology models). Negative correlations indicated, for example, that models with better performance projected later autumn phenology than models with poorer performance and vice versa. Second, we fitted GAMs per site- and per species-specific phenology model to the response variable Δ_{100} as described above (Supplement S5: Eq. S1) but excluded phenology models from the explanatory variables. We derived type-III ANOVA per GAM (Supplement S5, Eq. S14) and ranked the influence of (aggregated) optimization algorithms, sampling procedures, sample size proxies, and climate projection scenarios across phenology models. Thus, we calculated the Kendall rank correlation (Kendall, 1938) between these newly derived ranks and the ranks of the phenology models based on their effect on performance. In other words, we analyzed if the ranked aggregated influence of, for example, climate projection scenarios on Δ_{100} correlated with the ranked performance of phenology models. In this example, negative correlations indicated that climate projection scenarios had a larger relative influence on projected autumn phenology when combined with phenology models that performed better than with models that performed worse and vice versa. As before, each GAM and ANOVA was fitted and derived five times per phenology model and climate projection scenario based on five random samples of 10^5 corresponding projections per climate projection scenario. Therefore, the ranks of optimization algorithms, sampling procedures, sample size proxies, and climate projection scenarios were based on the mean coefficient estimates or mean relative explained variance.

We chose a low significance level and specified Bayes factors, to account for the large GAMs with many explanatory variables and the frequent mis- or overinterpretation of *p*-values (Benjamin and Berger, 2019; Goodman, 2008; Ioannidis, 2005; Wasserstein et al., 2019; Nuzzo, 2015). We applied a lower than usual significance level, namely $\alpha = 0.01$ (i.e. $p < 0.005$ for two-sided distributions; Benjamin and Berger, 2019), and included the 99% confidence intervals in our results. In addition, we complemented the *p*-values with Bayes factors (BF) to express the degree to which our data changed the odds between the respective null and alternative hypothesis (BF01; Johnson, 2005; Held and Ott, 2018). For example, if we assume a prior probability of 20% for the alternative hypothesis (i.e. a prior odds ratio H0:H1 of 80/20 = 4/1), then a BF_{01} of 1/20 means that the new data suggests a posterior odds ratio of 1/5 (i.e. 4/1 × 1/20) and thus a posterior probability of 83.3% for the alternative hypothesis. Our study was exploratory in nature (Held and Ott, 2018, Sect. 1.3.2), hence our null hypothesis was that there is no effect as opposed to the alternative hypothesis that there is one, for which a local distribution around zero is assumed (Held and Ott, 2018, Sect. 2.2). We derived the corresponding sample-size adjusted *minimum* BF_{01} ($\underline{BF}_{01}$) from the *p*-values of the GAM coefficients, ANOVA, and Kendall rank correlations (Johnson, 2005, Eq. 8; Held and Ott, 2016, Sect. 3; 2018, Sect. 3). While BF_{01} never exceed the value of 1, BF_{01} below 1/100 may be considered "very strong" and BF_{01} above 1/3 may be (very)

https://doi.org/10.5194/egusphere-2022-1423
Preprint. Discussion started: 31 January 2023

"weak" (Held and Ott, 2018, Table 2). Hence forward, we refer to results with $p < 0.005$ as significant and with $\underline{BF}_{01} < 1/1000$ as "decisive". Note that the $\underline{BF}_{01}$ expresses the most optimistic shift towards the alternative hypothesis.

All computations for data preparations, calculations, and visualizations were conducted in R (versions 4.0.2 and 4.1.3 for scientific computing and data visualisations, respectively; R Core Team, 2022) with different packages: Data were prepared with data.table (Dowle and Srinivasan, 2021), phenology models were coded based on phenor (Hufkens et al., 2018) and calibrated with DiceDesign and DiceOptim (for the optimisation algorithms EGO and TREGO; Dupuy et al., 2015; Picheny et al., 2021), GenSA via phenor (GenSA; Xiang et al., 2013; Hufkens et al., 2018), pso (PSO; Bendtsen, 2012), and cmaes (CMA-ES; Trautmann et al., 2011), while the RMSE was calculated with hydroGOF (Zambrano-Bigiarini, 2020). The formulas for the GAMs were translated from linear mixed-effects models with buildmer (Voeten, 2022), GAMs were fitted with mgcv::bam (Wood, 2011, 2017), the corresponding coefficients and *p*-values were extracted with mixedup (Clark, 2022), and sample size-adjusted $\underline{BF}_{01}$ were derived from *p*-values with pCalibrate::tCalibrate (Held and Ott, 2018). Summary statistics, ANOVA, and correlations with respective p-values were calculated with stats (R Core Team, 2022). Figures and tables were produced with ggplot2 (Wickham, 2016), ggpubr (Kassambara, 2020), and gtable (Wickham and Pedersen, 2019).

3 Results

3.1 Model performance

We evaluated 2 217 888 and 139 231 externally validated site- and species-specific calibration runs. Each of these runs represented a unique combination of 21 models, 10 optimization algorithms, 7 calibration samples × 500 sites with the site-specific calibration or 9 calibration samples with the species-specific calibration, and 3 species. All samples for the species-specific calibration were drawn 5 times except for the full sample. From the initial site- and species-specific calibration runs, 136 500 and 7 048 runs, respectively, did not converge, while another 373 126 and 12 524 runs led to NA values in either the internal or external validation (Supplement S6: Fig. S1).

3.1.1 Observed effects

Across the phenology models, optimization algorithms, and sampling procedures, the observed distribution of the external root mean square error (RMSE) of the pooled species differed considerably between the calibration and validation modes. Overall, the smallest median RMSEs were similar between the site- and species-specific calibration modes, ranging from 10.1 to 12.4 and 11.7 to 12.6 or 12.4 to 12.9 days in the respective site- and species-specific calibration validated within sample or within population (Fig. 2, Supplement S6: Table S1). Surprisingly, the smallest mean RMSE were considerably larger with the site- than with the species-specific calibration (19.2–52.1 vs. 11.6–23.9 or 12.9–24.4 days; grey dots in Fig. 2). Accordingly, standard deviations were larger with the site- than with the species-specific calibration (28.4–66.5 vs. 3.7–36.6 or 1.2–36.0 days; Fig. 2, Supplement S6: Table S1).

https://doi.org/10.5194/egusphere-2022-1423
Preprint. Discussion started: 31 January 2023

In the site-specific calibration, increasing sample size relative to the number of free model parameters (N:q) first lowered and then increased the RMSE and generally decreased the bias-variance trade-off. Binned mean RMSE and corresponding standard deviations ranged from 35.8 to 61.1 and from 58.5 to 71.9 days, respectively (Fig. 3c; Supplement S6: Table S2). The binned mean RMSE ratio regarding the bias-variance trade-off (i.e. external RMSE:internal mean RMSE) decreased steadily from 1.5 to 1.0 and at decreasing step sizes with bins of increased N:q. Step sizes between binned N:q were considerably larger for N:q < 9.4 than for N:q ≥ 11.8 (Supplement S6: Table S2) and we observed an abrupt increase in the scatter of the RMSE and RMSE ratio below an N:q of ~9 (Fig. 3c).

In species-specific calibration, larger sample sizes generally co-occurred with smaller population RMSE and higher degrees to which a model represented the population, except for the stratified samples, which led to the best modelled phenology at the population level and the highest degree of population representation. The mean population RMSE and corresponding standard deviation ranged from 24.4 to 30.2 and 36.0 to 40.4 days (Fig. 3d; Supplement S6: Table S2). We observed the smallest mean population RMSE in the stratified sample based on average mean annual temperature (MAT; 12 sites; RMSE = 24.4), followed by the stratified sample based on average autumn phenology (AP; 17 sites; RMSE = 25.9 days), and the full sample (500 sites; RMSE = 25.9 days). Except for the stratified samples, increasing sample size resulted in a steady increase in the RMSE ratio regarding the degree to which a model represents the population, which indicated a generally better representation of the population with larger samples. The ratio for stratified MAT samples followed just behind that of the full sample and was 0.95, followed by the samples with 200 and 100 sites that led to a ratio of 0.94. The ratio for the stratified AP samples even exceeded that of the full sample and was 1.21 (i.e. the validation within the samples led to larger RMSE than the validation within the population). Thus, the most accurate modelling of autumn phenology at the population level was achieved with stratified MAT samples rather than with the full sample. Furthermore, models calibrated with AP samples performed better when applied to the whole population, suggesting that the population is better represented with AP samples than with the full sample.

https://doi.org/10.5194/egusphere-2022-1423
Preprint. Discussion started: 31 January 2023

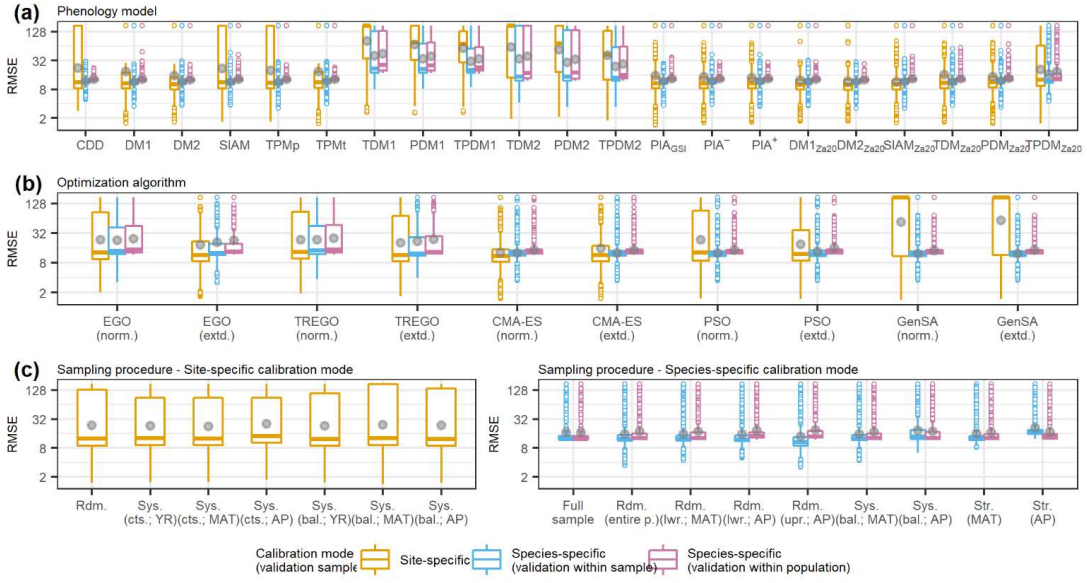

Figure 2: Observed distributions of the external root mean square error (RMSE) of the pooled species according to (a) phenology models, (b) optimization algorithms, and (c) sampling procedures. The thick horizontal lines and grey dots indicate the respective median and mean. Boxes cover the inner quartile range, whiskers extend to the most extreme observations or to 1.5 times the inner quartile range, and outliers are indicated as colored circles. Note that the y-axes were log-transformed. In all figures, the colors represent the calibration and validation modes. The abbreviations for the models, algorithms, and sampling procedures are explained in respective Tables Supplement S2: Table S1, Supplement S4: Table S1, and Supplement S4: Table S2/S3.

https://doi.org/10.5194/egusphere-2022-1423
Preprint. Discussion started: 31 January 2023

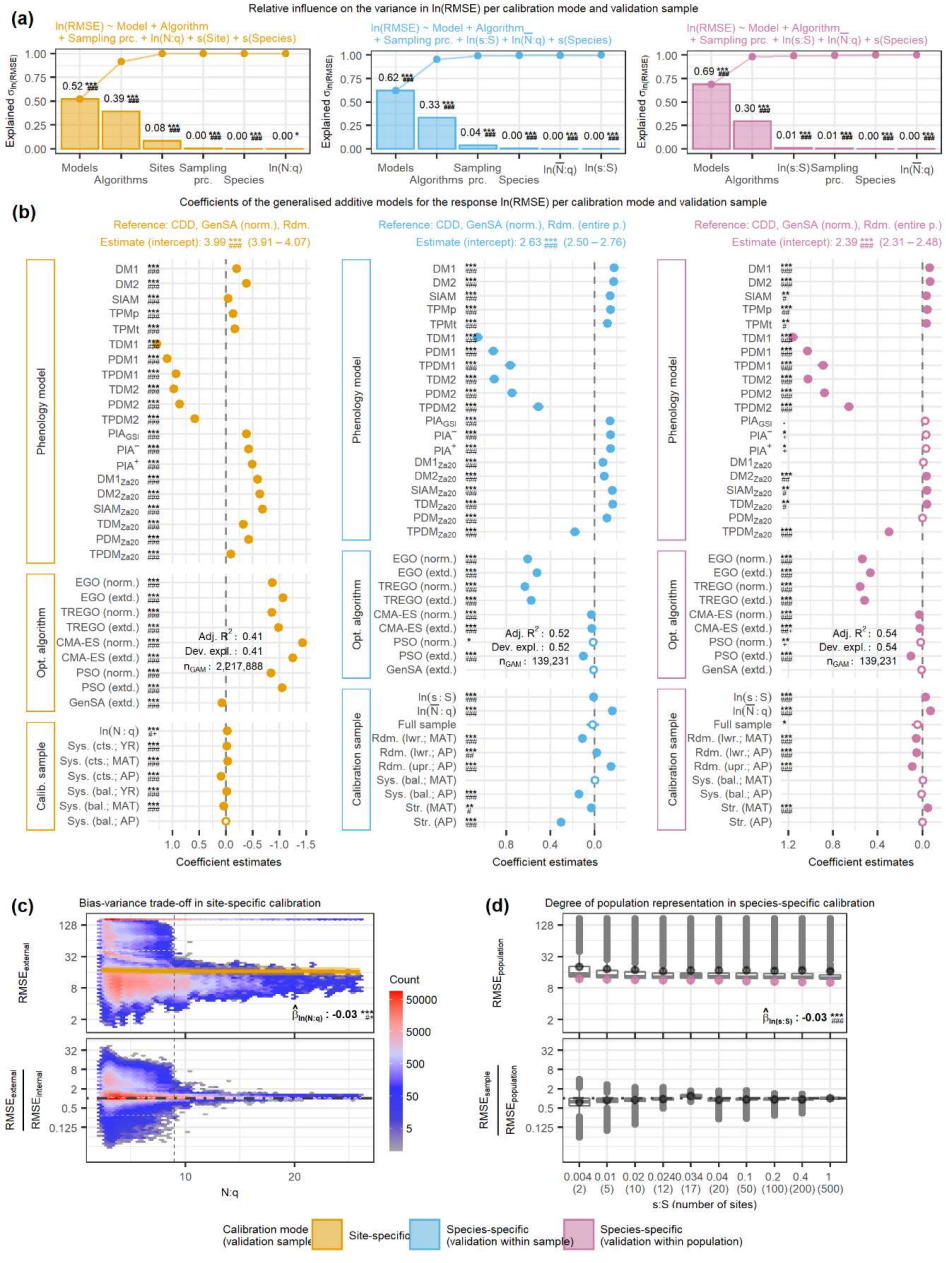

https://doi.org/10.5194/egusphere-2022-1423
Preprint. Discussion started: 31 January 2023

Figure 3: The relative variance in the log-transformed external root mean square error (RMSE) explained by phenology models, optimization algorithms, and calibration samples (i.e. sampling procedures and sample size proxies) together with the effects of the individual factors and the observed distribution of the RMSE according to sample size proxies. The relative variance was estimated from analyses of variance (a) based on generalized additive models (GAM; b) for site-specific calibration (left) as well as for within-sample validated (middle) and within-population validated (right) species-specific calibration. Observed distribution is plotted against (c) the number of observations per free model parameter (N:q) and (d) and the number of sites relative to the 500 sites of the entire population (s:S), illustrating the bias-variance trade-off with site-specific calibration and the degree to which a model represents the population with species-specific calibration, respectively. In (a), the bars indicate the estimated influence of phenology models, optimization algorithms, sampling procedures, and sample size proxies (N:q, $\bar{N}$:q, and s:S) as well as of the random effects sites and species on the variance in RMSE. The connected dots show the cumulated influence. (b) shows the coefficient estimates (dots or circles) of the GAM together with their 0.5–99.5% confidence intervals (whiskers) on an inverted x-axis. Dots represent significant ($p < 0.005$) coefficients. Significance levels of each coefficient are indicated with ., *, **, or *** corresponding to $p < 0.1$, 0.05, 0.01, or 0.001, respectively. Further, the minimum Bayes factor is indicated with +, #, #+, ##, ##+, or ### corresponding to $\underline{BF}_{01} < 1/3$, 1/10, 1/30, 1/100, 1/300, or 1/1000, respectively. Adjusted R^2 and deviance explained are printed (*Adj. R2* and *Dev. expl.*, respectively). Note, that negative coefficients (i.e. to the right of the dashed black line) indicate lower RMSE and thus better model performance. In (c), the observed distribution of the actual (top) and relative (bottom) external RMSE are plotted against N:q. The color of the hexagons represents the respective number of observations within the area they cover, and the dashed black line indicates N:q = 9. For the actual RMSE, the estimated size effect according to the GAM is plotted with a solid golden line (median) and a golden shaded area (0.5–99.5% confidence interval). For the relative RMSE, the external RMSE is larger than the internal RMSE in observations above the dot-dashed black line and vice versa. In (d), the observed distribution of the actual (top) and relative (bottom) external population RMSE are plotted for each s:S. For the actual RMSE, the estimated size effect according to the GAM is plotted with purple dots (median) and purple whiskers (0.5–99.5% confidence interval). For the relative RMSE, the external population RMSE is larger than the external sample RMSE in observations above the dot-dashed black line and vice versa. In (c) and (d), the printed values of the corresponding coefficient estimates ($\widehat{\boldsymbol{\beta}}$) refer to the log-transformed RMSE and respective N:q or s:S. The abbreviations for the models, algorithms, and sampling procedures in all figures are explained in respective Tables Supplement S2: Table S1, Supplement S4: Table S1, and Supplement S4: Table S2/S3.

3.1.2 Estimated effects

The evidence in the analyzed data against H0 was significant and decisive for the estimated effects ($p < 0.005$ and $\underline{BF}_{01} < 1/1000$) and aggregated influences ($p < 0.01$ and $\underline{BF}_{01} < 1/1000$) of most factors, while the deviances explained ranged from 0.41 to 0.67 (Fig. 3, Supplement S6: Fig. S4, Supplement S6: Tables S8–S11 and S15–S18).

Phenology models had generally the largest influence on model performance among optimization algorithms, sampling procedures, sample size, sites, and species, but the degree of influence as well as the best performing models depended on the calibration mode (Fig. 3, Supplement S6: Table S5–S8). Aggregated phenology models explained 52% and 62% or 69% of the variance in RMSE in the site- and species-specific calibration when validated with the sites of the sample or the entire population, respectively (Fig. 3, Supplement S6: Table S8). We estimated the effect on the RMSE of each model relative to the reference CDD model and per calibration mode. In the site-specific calibration, the effects were generally larger than in the species-specific calibration (Fig. 3, Supplement S6: Table S9–S11). Further, the ranks of the models according to their effects differed between calibration modes (Fig. 3, Supplement S6: Table S5–S7).

In the site-specific calibration, all 20 phenology models had decisive and significant effects on the RMSE of the reference CDD model, which ranged from halving to tripling, and their ranking depended strongly on the treatment of NA values and non-converging runs (Fig. 3 and Supplement S6: Fig. S4, Supplement S6: Tables S5 and S12). The reference model CDD led to an RMSE of 49.8–58.6 days in site-specific calibration (99% confidence interval, CI_{99}; see Supplement S5: Sect. 3 for the back-transformation of the coefficient estimates; Fig. 3, Supplement S6: Tables S5 and S9). The largest reduction from this RMSE was achieved with the models $SIAM_{Za20}$, $DM2_{Za20}$, $DM1_{Za20}$, and PIA^{+}, ranging from -50% to -39% (CI_{99}). Model ranks

https://doi.org/10.5194/egusphere-2022-1423
Preprint. Discussion started: 31 January 2023

and effect sizes changed considerably if NA-producing and non-converging calibration runs were excluded: The RMSE of the reference model CDD dropped to 6.0–7.6 days (CI_{99}) and was not reduced by any of the other models (Supplement S6: Fig. S4, Supplement S12: Table S16). In other words, if only calibration runs without NAs were considered, the CDD model performed best, followed by SIAM, $DM2_{Za20}$, and TPMp.

In the species-specific calibration, all 20 or 9 models had decisive and significant effects compared to the reference model CDD if validated within sample or population, respectively, with effects ranging from a reduction by one-fifth to a tripling and resulting in fairly consistent model ranks between the two NA treatments (Fig. 3, Supplement S6: Fig. S4, Supplement S6: Tables S6–S7 and S13–S14). The RMSE according to the reference model CDD was 12.1–15.7 or 10.0–11.9 days (CI_{99}) if validated within sample or population, respectively (Fig. 3, Supplement S6: Table S6–S7 and S10–S11). According to the within-sample validation, the RMSE was reduced the most with the DM1, DM2, TDM_{Za20}, and $SIAM_{Za20}$, with reductions between -16% and -15% (CI_{99}). According to the within-population validation, the models DM2, DM1, TPMp, and TDM_{Za20} reduced the RMSE the most and reductions ranged from -10% to -1% (CI_{99}; Fig. 3, Supplement S6: Tables S6–S7 and S10–S11). If NA-producing and non-converging runs were excluded, the reference RMSE increased to 16.2–20.2 or 12.9–13.9 days (CI_{99}; validated within sample or population, respectively), while model ranks were changed in two positions (Supplement S6: Fig. S4, Supplement S6: Tables S13–S14).

Optimization algorithms had the second largest influence on model performance, explaining about one-third of the variance in RMSE, with differences between the calibration modes and NA treatments regarding degree of influence and ranking of individual algorithms (Fig. 3, Supplement S6: Fig. S4, Supplement S6: Tables S5–S8 and S12–S15). Aggregated algorithms explained 39% and 33% or 30% of the variance in RMSE in site- and species-specific calibration validated within sample or population, respectively (Fig. 3, Supplement S6: Table S8). In the site-specific calibration, both CMA-ES algorithms (norm. and extd.) resulted in the smallest RMSEs, which were -76% to -71% (CI_{99}) lower than the RMSE according to the reference GenSA (norm.; CI_{99} of 49.9–58.6 days, see above; Fig. 3, Supplement S5: Table S5 and S9). In species-specific calibration, the best results were obtained with both GenSA algorithms (norm. and extd.), whereas the Bayesian algorithms (EGO and TREGO, norm. and extd.) performed worst and resulted in RMSEs +57% to +91% (CI_{99}) larger the RMSE according to the reference RMSE (CI_{99} of 12.1–15.7 or 10.0–11.9 days if validated within sample or population, see above; Fig. 3, Supplement S6: Tables S6–S7 and S10–S11). If NA-producing and non-converging calibration runs were excluded, the lowest and largest RMSEs with site-specific calibration were obtained with the GenSA and the Bayesian algorithms, respectively. With species-specific calibration, we observed little change when only calibration runs without NAs were analyzed: As before, Bayesian algorithms led to the largest RMSEs, while both GenSA algorithms resulted in the smallest RMSEs (Supplement S6: Fig. S4, Supplement S6: Tables S12–S14).

Sampling procedures had little influence on model performance in general (third or fourth largest) and were more important with species- than with site-specific calibration where stratified sampling procedures led to the best results (Fig. 3, Supplement S6: Tables S5–S8). Aggregated sampling procedures explained 0.3% and 4.0% or 0.7% of the variance in RMSE with site- and species-specific calibration validated within sample or population, respectively (Fig. 3, Supplement S6: Table S8). With

https://doi.org/10.5194/egusphere-2022-1423
Preprint. Discussion started: 31 January 2023

site-specific calibration, systematically continuous samples based on mean annual temperature (MAT) and year performed best, diverging by -4.3% to -1.3% (CI_{99}, Fig. 3, Supplement S6: Table S5 and S9) from the RMSE according to the reference random sampling. With species-specific calibration, we received the lowest RMSEs with random samples from half of the population (split according to MAT or autumn phenology) when validated within sample (Fig. 3, Supplement S6: Tables S6 and S10). When validated within population, stratified samples based on MAT performed best, diverging by -6.9% to -2.3% (CI_{99}) from the RMSE according to the reference random sampling from the entire population (Fig. 3, Supplement S6: Tables S7 and S11). The alternative NA treatment had little effect on these results in general but led to an influence of 49% of sampling procedures with species-specific calibration validated within sample, while systematically balanced samples performed best with site-specific calibration (Supplement S6: Fig. S4, Supplement S6: Tables S12–S15). Note that for the site-specific calibration, these sampling procedures refer to the allocation of observations for the 5-fold cross-evaluation, whereas for the species-specific calibration they refer to the selection of sites.

Sample size effects on model performance were very small but showed that more observations per free model parameter led to smaller RMSE, except with site-specific calibration when NA-producing runs were excluded (Fig. 3, Supplement S6: Fig. S5, Supplement S6: Tables S5–S8 and S12–S15). Among the size proxies relative (average) number of observation (N:q or $\bar{N}$:q) and site ratio (s:S), only s:S with species-specific calibration validated within population explained more than 0.15% of the variance in RMSE, namely 1.0% (Fig. 3, Supplement S6: Table S8). An increase of 10% in N:q reduced the RMSE by approximately -0.5% to -0.1% with site-specific calibration, while an increase of 10% in the $\bar{N}$:q led to reductions of approximately -1.8% to -1.2% or -1.0% to -0.4% (CI_{99}) with respective species-specific calibration validated within sample or population (Supplement S6: Table S5–S7). A 10% increase in s:S with species-specific calibration increased the RMSE by +0.08% to +0.13% (CI_{99}) if validated within sample and decreased it by -0.30% to -0.26% (CI_{99}) if validated within population (Supplement S6: Table S6 and S7). By excluding NA-producing and non-converging runs, a 10 % increase in N:q increased the RMSE in site-specific calibration by +0.4 to +0.6% (CI_{99}; Supplement S6: Fig. S4, Supplement S6: Tables S12–S15).

Sites and species were included as grouping variables for the random effects and had little influence on model performance, except for sites with site-specific calibration. Sites explained 8.4% of the variance in RMSE with site-specific calibration and hence had a larger influence than sampling procedure and sample size (i.e. N:q) combined (Fig. 3, Supplement S6: Table S8). Species only explained more than 0.1% of the variance in species-specific calibration validated within sites, namely 0.4%. Thus, species had a slightly greater influence than $\bar{N}$:q and s:S combined (Fig. 3, Supplement S6: Table S8). When only converged calibration runs without NAs were analyzed, sites became the second most important driver of the variance in RMSE in site-specific calibration, explaining 27% (Supplement S6: Fig. S4, Supplement S6: Table S15).

3.2 Model projections

We analyzed the effects on the 100-year shifts at site-level (Δ_{100}) in autumn phenology projected with site- and species-specific models within sample or population and based on five random samples per projection mode. Each sample consisted of 10^5 projected shifts per climate projection scenario, i.e. 2.6×10^6 projected shifts per sample, which were drawn from

https://doi.org/10.5194/egusphere-2022-1423
Preprint. Discussion started: 31 January 2023

corresponding datasets that consisted of >4.1×10^7 and >1.9×10^8 or >1.5×10^9 Δ_{100} projected with site- and species-specific phenology models for the sites within sample or population, respectively. These datasets were based on 16 climate model chains (CMC) based on the representative concentration pathway 4.5 (RCP 4.5), and 10 CMC based on RCP 8.5. The analyzed data (i.e. 3.9×10^7 Δ_{100}) provided significant and decisive evidence against H0 for most estimated effects and most aggregated influences (Fig. 4, Supplement S6: Tables S22–S25).

https://doi.org/10.5194/egusphere-2022-1423
Preprint. Discussion started: 31 January 2023

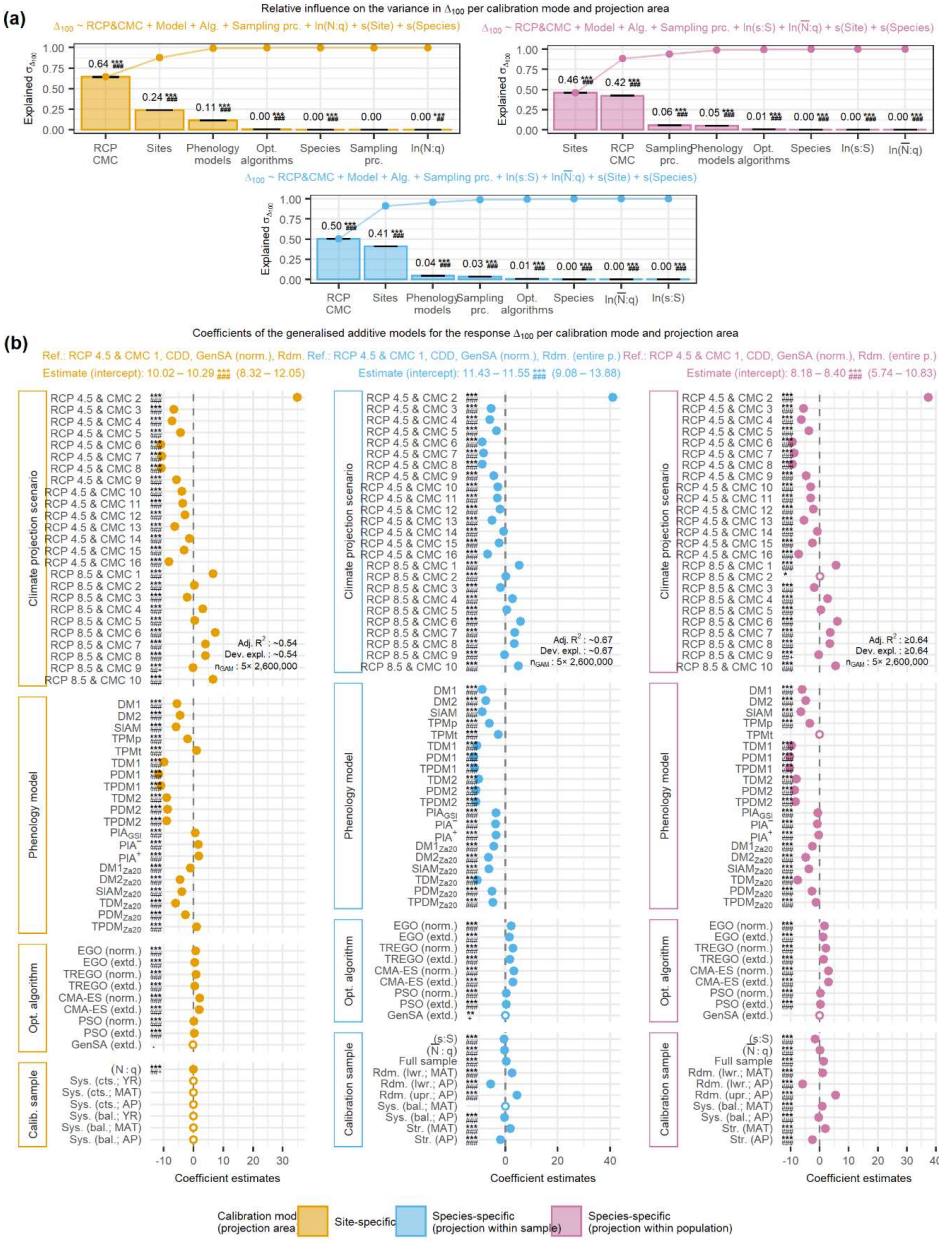

https://doi.org/10.5194/egusphere-2022-1423
Preprint. Discussion started: 31 January 2023

Figure 4: The relative variance in the projected 100-year shifts at site-level (Δ_{100}) of autumn phenology and corresponding effects explained by climate projection scenarios (i.e. representative concentration pathways, RCP, and climate model chains, CMC), phenology models, optimization algorithms, and calibration samples (i.e. sampling procedures and sample sizes). The relative variance was estimated from analyses of variance (a) based on generalized additive models (GAM; b) for Δ_{100} according to site-specific models (left) as well as according to species specific models when projected within sample (middle) or within population (right). In (a), the black error-bars indicate the range of estimated influence from the five GAM based on random samples. In (b), the median coefficient estimates from the five GAMs are visualized. If all five estimates were significant ($p < 0.005$), the median is indicated with a dot and with a circle otherwise. None of the 99% confidence intervals from any of the five GAMs extended beyond either dot or circle and are thus not shown. Note that coefficients estimate the difference to the reference Δ_{100}. Thus, a negative coefficient estimate may indicate a projected advance or delay in autumn phenology, depending on how it relates to the reference. The abbreviations for the climate projection scenarios, phenology models, optimization algorithms, and sampling procedures in all figures are explained in respective Tables Supplement S1: Table S5, Supplement S2: Table S1, Supplement S4: Table S1, and Supplement S4: Table S2/S3. For a further description, see Fig. 3a and 3b.

3.2.1 Estimated effects

Climate projection scenarios had the largest and second largest influence on projected autumn phenology in general, and the warmer RCP 8.5 caused larger shifts than the cooler RCP 4.5. Aggregated climate projection scenarios (i.e. unique combinations of RCP and CMC) explained between 46% and 64% of the variance in Δ_{100} in all projections (Fig. 4, Supplement S6: Table S22). The Δ_{100} according to site-specific models was +10.0 to +10.3 days (CI_{99}) based on the reference RCP 4.5 & CMC 1. This base Δ_{100} was altered between -11.1 to -11.0 days and ~-1.4 days (CI_{99}) by the RCP 4.5 scenarios, whereas the RCP 8.5 scenarios changed it by between -2.2 to -2.1 and +7.3 to +7.4 days (CI_{99}; except for the RCP 4.5 and CMC 2, which altered base Δ_{100} by +34.7 to +35.0 days, CI_{99}; Fig. 4, Supplement S6: Tables S19 and S23). The Δ_{100} according to species-specific models ranged from +11.4 to +11.6 days (CI_{99}) or from +8.2 to +8.4 days (CI_{99}) based on the reference RCP 4.5 and CMC 1 in respective projections within sample or within population (Fig. 4, Supplement S6: Tables S20, S21, S24, and S25). These base Δ_{100} were altered between -8.8 to -8.7 days and ±0.0 days (CI_{99}) or between -9.4 to -9.2 days and ±0.0 days (CI_{99}) by the RCP 4.5 scenarios, in corresponding projections within sample or within population (except for RCP 4.5 and CMC 2, which altered base Δ_{100} by >+37.1 days). The RCP 8.5 scenarios changed the base Δ_{100} projected within sample or within population by between -1.8 to -1.7 days and +5.8 to +6.0 days (CI_{99}) or between -2.0 to -1.8 days and +6.1 to +6.2 days (CI_{99}), respectively.

When analyzed per phenology model, climate projection scenarios exhibited the largest influence on autumn phenology projected by over one-third of the models. Across the site-specific models, aggregated climate projections were most influential on Δ_{100} for 13 models and the largest fractions were observed for the models DM2 (76%) and $DM2_{Za20}$ (69%; Supplement S6: Fig. S6; Supplement S6: Table S27). Across the species-specific models, aggregated climate projections within sample or population were most influential on Δ_{100} for 12 or 8 models, respectively, and the largest fractions were observed for the models DM2 (49% or 58%) and $DM2_{Za20}$ (49% or 56%; Supplement S6: Fig. S7 and S8; Supplement S6: Tables S28 and S29). Phenology models had the third and fourth largest influence on projections of autumn phenology according to site- and species-specific models, respectively, while TDM, PDM, and TPDM models generally projected the most pronounced forward shifts and CDD, TPMt and PIA models the most pronounced backward shifts. Aggregated phenology models explained 11% and 4% or 5% of the variance in Δ_{100} when projected with site- and species-specific models within sample or population,

https://doi.org/10.5194/egusphere-2022-1423
Preprint. Discussion started: 31 January 2023

630 respectively (Fig. 4, Supplement S6: Table S22). When projected by site-specific models, the Δ_{100} based on the reference CDD model was reduced the most with the PDM1, TPDM1, and TDM1 models (from -11.8 to -9.8 days; CI_{99}; Fig. 4, Supplement S6: Tables S19 and S23). The largest increases occurred with the PIA^{+}, PIA^{-}, $TPDM_{Za20}$ models (from +0.9 to +1.8 days, CI_{99}). When projected with species-specific models, the Δ_{100} based on the reference CDD model was reduced with all other models (Fig. 4, Supplement S6: Tables S20, S21, S24, and S25). Here, the largest reductions occurred with the PDM1, TPDM1, and
635 PDM2 or TDM1 models (from -12.0 to -11.2 or from -10.4 to -9.7 days; CI_{99}), while the least reductions occurred with the PIA^{-}, PIA^{+}, PIA_{GSI}, and TPMt models (from -3.8 to -2.6 days or from -0.8 to -0.1 days, if projected within sample or population respectively; CI_{99}).

Optimization algorithms had little influence on projections in general, while the algorithms CMA-ES (norm. and extd.) and TREGO (norm.) led to largest deviations from the reference. Aggregated optimization algorithms explained less than 1% of
640 the variance in Δ_{100} according to either site- or species-specific models (Fig. 4, Supplement S6: Table S22). When projected with site-specific models, the Δ_{100} according to the reference GenSA (norm.) was only reduced by the GenSA (extd.; ~-0.1 days; CI_{99}) algorithm and increased most, namely between +0.9 and +2.1 days (CI_{99}), by both CMA-ES and the TREGO (norm.) algorithms (Fig. 4, Supplement S6: Tables S19 and S23). When based on species-specific models, the lowest Δ_{100} was obtained with the reference. Again, both CMA-ES and the TREGO (norm.) algorithms increased Δ_{100} the most compared to
645 the reference, namely from +3.0 to +3.3 days or +2.1 to +3.1 days (CI_{99}) in projections within sample or within population (Fig. 4, Supplement S6: Tables S20, S21, S24, and S25).

Sampling procedures had by definition no influence on projections with site-specific models and the third or fourth largest influence on projections with species-specific models. Since site-specific model parameters for projections were calibrated with all observations per site, effects of corresponding sampling procedures on Δ_{100} would be random. Subsequently, our
650 results indicated no general (i.e. according to *all* five samples) significant or decisive effect of any sampling procedure (Fig. 4, Supplement S6: Table S23). However, the *p*-values of two sampling procedures fell below the significance level according to at least one of the five GAMs, leading to a type I error or "false positive", whereas none of the GAMs resulted in a decisive influence according to the Bayes factor. In projections with species-specific models, sampling procedures had an influence and explained 3% or 6% of the variance in Δ_{100} when projected within site or within population (Fig. 4, Supplement S6: Table
655 S22). In comparison to the reference random sample from the entire population, Δ_{100} was reduced or increased the most when projections were based on random samples from the lower or upper half of the population according to average autumn phenology, respectively (Fig. 4, Supplement S6: Tables S20, S21, S24, and S25). Corresponding effect sizes were ~-5.6 days or ~+4.5 days and -5.9 to -5.8 days or +5.4 to +5.5 days (CI_{99}) when projected within sample and within population, respectively.

660 Sample size proxies had the smallest influence. Neither N:q and $\bar{N}$:q nor the site ratio (s:S) explained more than 0.5% of the variance in Δ_{100} (Fig. 4, Supplement S6: Table S22). In projections with site-specific models, effects were ~+0.0 days for N:q (CI_{99}; Fig. 4, Supplement S6: Tables S19 and S23). In projections with species-specific models, the effects were ~+0.2 days

https://doi.org/10.5194/egusphere-2022-1423
Preprint. Discussion started: 31 January 2023

or ~+0.1 days for $\bar{N}$:q (CI_{99}) when projected within sample and within population, respectively, and +0.0 days for s:S (CI_{99}; Fig. 4, Supplement S6: Tables S20, S21, S24, and S25).

Sites were the most and second most important driver of autumn phenology projected with both site- and species-specific models, while the influence of species was very low. Sites explained 24% and 41% or 46% of the variance in Δ_{100} when projected with site- and species-specific models within samples or population, respectively (Fig. 4, Supplement S6: Table S22). Species accounted for less than 0.5% of the variance in Δ_{100} projected with either site- or species-specific models.

3.2.2 Relations with model performance

Coefficient estimates for performance and projections were negatively correlated across phenology models and positively correlated across optimization algorithms for both site- and species-specific models, but with neither decisive nor significant evidence. With site-specific calibration and projection, we derived the highest Kendall rank correlations for sampling procedures with $\tau = +0.71$ ($p = 0.024$ and $\underline{BF}_{01} = 1/5.1$) and weaker negative and positive correlations for phenology models and optimization algorithms, respectively (Fig. 5, Supplement S6: Table S26). With species-specific calibrations and projections, the correlations for phenology models and sampling procedures were negative, whereas those for optimization algorithms were positive. When projected within sample or population, the strongest correlations were derived for optimization algorithms or for phenology models, namely $\tau = -0.50$ or $\tau = -0.35$ ($p = 0.061$ and $\underline{BF}_{01} = 1/2.2$ or $p = 0.032$ and $\underline{BF}_{01} = 1/3.1$), respectively (Fig. 5, Supplement S6: Table S26). Thus, while the best performing phenology models were related to larger Δ_{100}, the best performing optimization algorithms were associated with smaller Δ_{100}, without any regularity in sampling procedures. In other words, autumn phenology was projected to occur later if based on better performing models.

Projections with site-specific models were influenced more by climate projection scenarios and less by sites when based on better performing phenology models. The evidence was strongest for the correlations between the performance rank of phenology models and the relative influence of climate projection scenarios on the variance in Δ_{100} ($\tau = -0.64$; $p < 0.005$ and $\underline{BF}_{01} = 1/788$) or sites ($\tau = +0.59$; $p < 0.005$ and $\underline{BF}_{01} = 1/249$; Fig. 5, Supplement S6: Fig. S5 and S6, Supplement S6: Table S26). This suggests that the better the underlying models performed, the more closely the projections of autumn phenology followed the climate signal, and vice versa. Also, the better the underlying models performed, the more the projections of autumn phenology became detached from the sites.

Projections with species-specific models and within population were a little more influenced by climate projection scenarios and less influenced by optimization algorithms when based on better performing models, whereas the influence of (aggregated) factors on projections within sample appeared to be unrelated to model performance. When projected within population, the evidence was strongest for the correlations between performance rank of models and climate projection scenarios ($\tau = -0.32$; $p = 0.040$ and $\underline{BF}_{01} = 1/2.6$) or optimization algorithms ($\tau = +0.34$; $p = 0.030$ and $\underline{BF}_{01} = 1/3.3$; Fig. 5, Supplement S6: Fig. S5, S7, and S8, Supplement S6: Table S26). That is, the better the models are, the more the projections depended on the climate signal and the less they were influenced by the optimization algorithm.

https://doi.org/10.5194/egusphere-2022-1423
Preprint. Discussion started: 31 January 2023

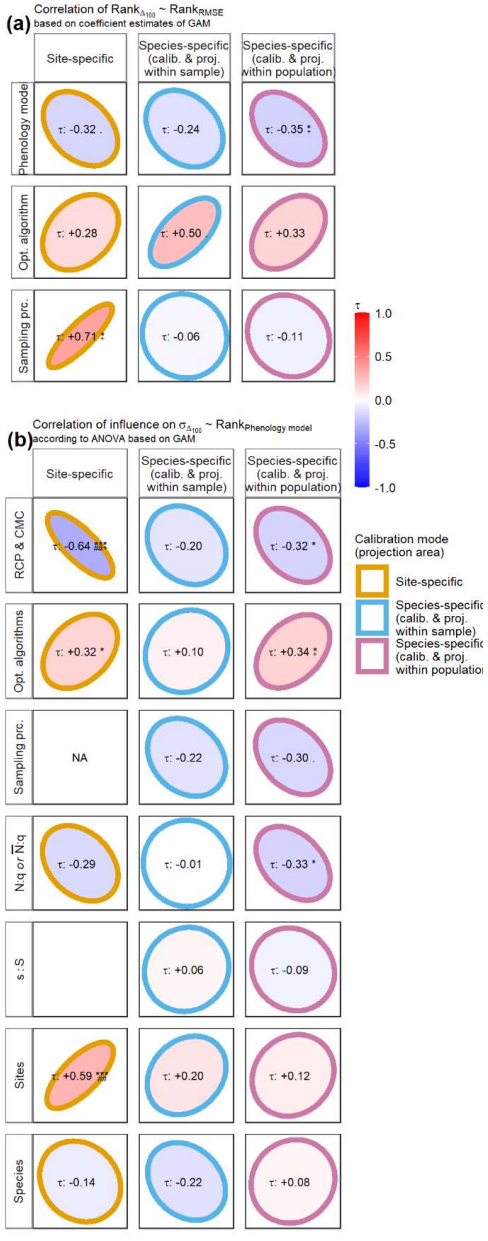

https://doi.org/10.5194/egusphere-2022-1423
Preprint. Discussion started: 31 January 2023

Figure 5: Kendall rank correlation (τ) between coefficient estimates of explanatory variables for log-transformed root mean square error (RMSE) and 100-year shifts (Δ_{100}) at site-level (a) and between coeffiecient estimates of phenolgy models for log(RMSE) and the relative influence on the variance in Δ_{100} of the remainng factors (b). The colour of the ellipses corresponds to the calibration mode and corresponding projections, whereas their filling visualises the value of τ. The value of τ is further expressed by the angle (negtive vs. postive) and length of minor axis (absolute value). Asterisks and dots refer to the *p*-value, while hashtags and crosses refer to the minimum Bayes factor (see Fig. 3 for further details).

4 Discussion

We evaluated the effects of phenology models, optimization algorithms, sampling procedures, and sample size on the performance of phenology models if calibrated per site (i.e. one set of parameters per species and per site) and per species (i.e. one set of parameters per species and for the entire population). The performance was mainly influenced by the phenology models, followed by the optimization algorithms. In general, simple phenology models that depended on daily temperature, day length, and partly on average seasonal temperature or spring leaf phenology performed best, and non-Bayesian optimization algorithms outcompeted the Bayesian algorithms. The entire population was best represented by species-specific phenology models calibrated with stratified samples that were based on equally sized bins according to the average phenology per site. Site- or species-specific models performed best when trained with systematically balanced or stratified samples based on mean annual temperature, respectively. The bias-variance trade-off with site-specific calibration increased considerably when the ratio of the number of observations relative to the number of the free model parameter fell below nine.

We further evaluated the effects of phenology models, optimization algorithms, sampling procedures, sample size, and climate projection scenarios on the projected 100-year shift in autumn leaf phenology according to site- or species-specific models. Projected autumn phenology generally shifted between –13 and +12 days or between –4 and +20 days according to the representative concentration pathway 4.5 or 8.5 (RCP 4.5 or RCP 8.5, respectively), depending on the scenario and phenology model and based on the reference optimization algorithm and sampling procedure. The shifts were mainly influenced by climate projection scenarios and sites. The relative influence of phenology models was surprisingly small, but shifts projected with better performing models were generally larger and depended more on projected climate change than shifts according to models with poorer performance.

4.1 Phenology models

Phenology models had the largest influence on model performance, which justifies inferences from comparisons of process-oriented models to the phenology-driving processes. In model comparisons, better performing models are usually accredited as being based on relevant and correctly interpreted processes (e.g. Delpierre et al., 2009; Keenan and Richardson, 2015; Lang et al., 2019; Zani et al., 2020). Here we show that phenology models exerted the largest influence on model performance of all the factors analyzed. This reinforces model comparisons as a means to identify relevant processes.

Relatively simple models driven by daily temperature, day length, and partly by seasonal temperature or spring leaf phenology performed best, which supports the findings of some but not all previous studies. Patterns in ranked coefficient estimates

https://doi.org/10.5194/egusphere-2022-1423
Preprint. Discussion started: 31 January 2023

730 generally showed that the models DM1 and DM2 developed by Delpierre et al. (2009) and the models $DM1_{Za20}$, $DM2_{Za20}$, TDM_{Za20}, and $SIAM_{Za20}$ adapted by Zani et al. (2020) performed best. These models are very similar to the models that Liu et al. (2020) adapted from Delpierre et al. (2009) and Caffarra et al. (2011), which performed best in their model comparison study. Further, the models DM1 and DM2 performed best in Delpierre et al. (2009). However, the models $DM1_{Za20}$, $DM2_{Za20}$, TDM_{Za20}, and $SIAM_{Za20}$ did not lead to the best results in Zani et al. (2020). Daily senescence rate in all these models depends
735 on daily temperature and day length, while the threshold is either a constant or linearly derived from the actual average temperature during the growing season or the site-anomaly of spring phenology. Interestingly, the best performing models in site-specific calibration were those adapted by Zani et al. (2020) such that the senescence rate was based on a sigmoid curve, which economized one free model parameter (Table 1 and Supplement S2: Table S1). We hypothesize that fewer parameters generally lead to an advantage with few training observations, which needs to be examined in more detail in further studies.
740 Finally, our study supports previous studies that have also demonstrated the superiority of models based on daily temperature, day length, seasonal temperature, and spring phenology, while weakening studies that claimed other models to be superior.

Sites had a relatively large influence on projections with species-specific models, and the number of sites per sample had a negative effect on the sample-level model performance of species-specific models, suggesting that the phenology models studied miss important driving processes. In particular, models based on senescence rates driven by temperature and day length
745 and a corresponding threshold may miss relevant drivers (e.g. Fu et al., 2014b). Recent models accounted for this and based their threshold for the senescence rate on spring phenology (SIAM model; Keenan and Richardson, 2015) or on seasonal drivers such as the average growing season temperature or accumulated apparent photosynthetic product (TDM or PIA models; Liu et al., 2019; Zani et al., 2020). However, Gill et al. (2015) and Chen et al. (2018) observed site-specific responses of leaf phenology to climate change, which could be due to site-specific soil properties (Arend et al., 2016), nutrient availability (Fu
750 et al., 2019), and adaptation (Peaucelle et al., 2019), which are not yet included in the current models. While models may generally consider such relevant but excluded drivers through differently calibrated parameters, e.g. through a sample-specific threshold constant, this is not possible to the same extent for species-specific models as for site-specific models. The less such consideration is possible, the closer the modelled values are to the mean observation of the calibration sample. Consequently, we expect (1) a larger effect of sites on projections based on species-specific rather than site-specific models and (2) an
755 increasing RMSE with more sites per sample. Here we observed both, i.e. the relative influence of sites on projections increased from 24% to 46% or 41% if based on site-specific models or species-specific models projected within sample or within the entire population, respectively. Moreover, the RMSE of species-specific models validated within sample increased with more sites as expressed by the site ratio s:S. This demonstrates that some relevant drivers of autumn leaf phenology are not yet considered in the evaluated process-oriented models.

760 **4.2 Optimization algorithms**

We generally obtained the best results with the GenSA algorithm and found the Bayesian algorithms ran in extensive mode outperformed those ran in normal mode, which suggests that further extended Bayesian algorithms may perform even better.

https://doi.org/10.5194/egusphere-2022-1423
Preprint. Discussion started: 31 January 2023

While simulated annealing and its derivatives have been the algorithms of choice in various studies that calibrated process-oriented models of tree leaf phenology (e.g. Chuine et al., 1998; Meier et al., 2018; Zani et al., 2020), one derivative, namely GenSA (Xiang et al., 2013), is further the default algorithm of the R package phenoR (Hufkens et al., 2018). In this study, GenSA generally delivered the best results, which confirmed this choice. However, our results depended on the control settings of the algorithms such as the number of iterations. The Bayesian algorithms EGO and TREGO always performed better when executed in extensive mode and may lead to better results if the iterations and/or the number of starting points were increased further.

However, more iterations did not lead to more accurate results for all optimization algorithms, which implies that careful parameter setting should not be underestimated, because it affects the results and should therefore be communicated. We basically applied off-the-shelf algorithms (Trautmann et al., 2011; Bendtsen, 2012; Xiang et al., 2013; Picheny and Ginsbourger, 2014; Dupuy et al., 2015; Hufkens et al., 2018), using the respective default configurations except for the control of the number of iterations, which we adjusted depending on the number of free model parameters to execute them in normal and extended mode (i.e. few and many iterations). Expecting that more iterations lead to better results, we were surprised to find that this was not always true. However, all studied algorithms sample solutions of the cost function by changing the free parameters in small steps. This step size depends, among others, on the search space and the number of iterations. In turn, the complexity of the cost function depends on the model and the number of free parameters. While many iterations lead to small steps and vice versa, small steps may cause the algorithm to get stuck in a local optimum whereas large steps may cause it to overstep the global optimum. In addition, larger samples and more free parameters are expected to lead to more local optima. Therefore, we strongly suggest that studies of process-based phenology models set and test the control parameters of the optimization algorithms in dependence of the models as well as communicate and discuss the applied settings.

4.3 Calibration samples

Stratified selected sites based on autumn phenology seemed to represent the population better than the population itself, which appears to be an artefact of a model bias towards the mean phenology and advocates corresponding samples as ideal candidates for model testing. We evaluated the degree to which species-specific phenology models represented the entire population according to the ratio of the external *sample* RMSE to the external *population* RMSE. This ratio lay above one for stratified samples based on autumn phenology. In other words, the external RMSE decreased when calculated for the entire 500 sites instead of the 17 sites. This finding can be explained by the fact that modelled values tend towards the mean predictand. Given such a tendency, the errors between modelled and observed values result in a U-shaped (i.e. convex) curve across the predictands (i.e. smaller errors for the mean predictand and larger errors for the extremes). Consequently, normally distributed predictands result in a smaller RMSE than for example uniformly distributed predictands because the former distribution accounts for relatively more small errors around the mean predictand than the latter. Here we argue that autumn phenology (i.e. the predictand) tends to follow a uniform distribution in stratified samples based on autumn phenology and normally distributed in the full sample. Further, the tendency of phenology models towards the mean observed phenology manifested in

https://doi.org/10.5194/egusphere-2022-1423
Preprint. Discussion started: 31 January 2023

smaller variances of modelled than observed phenology in Delpierre et al. (2009, Fig. 2), Keenan and Richardson (2015, Fig. 3), Lang et al. (2019, Fig. 4), Liu et al. (2019, Fig. 2), and Zani et al. (2020; Fig. 3D, only for some models). Thus, we suggest that our phenology models were biased towards the mean, too, which led to the seemingly better representation of the population by stratified samples based on autumn phenology. Moreover, we hypothesize that the RMSE ratio in the other samples did not exceed one because the distributions of autumn phenology tended towards normal in all these samples. Finally, it follows from the above line of thought that models with a tendency towards the mean predictand have an advantage over models without such a tendency when the RMSE is calculated from normally distributed observations (provided convex and uniform error curves cover the same area within the observation range). This seems to be a hindrance in the search for models that represent a population and thus should fit all observations equally. Therefore, we advocate the use of stratified samples based on autumn phenology to test and evaluate calibrated models at the population level.

Our results suggest the use of systematically balanced observations in cross-validation and of randomly selected sites from stratified bins based on mean annual temperature in species-specific modelling. Systematically continuous samples led to the best results of cross-validated models, if NA values and non-converging-runs were penalized and included, whereas they were outperformed by systematically balanced samples based on autumn phenology or year, if NA-producing and non-converging-runs were excluded. Thus, the exclusion of such runs benefitted the balanced samples and/or penalized the continuous samples. This may be the case when some balanced samples led to more NAs or non-converging calibration runs than the continuous samples and/or some continuous samples led to very small root mean square errors despite one or more NAs. Since the first possibility seems more likely, we suggest that the best cross-validations are obtained with systematically balanced observations based on phenology or year, but this may also lead to convergence problems. In addition, we studied the effects of site selection on model calibration. Not surprisingly, if validated within sampled sites, the best results were obtained with samples of more uniform phenological patterns, namely with randomly sampled sites from either half of the population according to autumn phenology. More interestingly, if validated within the sites of the entire population, models calibrated with 12 randomly selected sites from stratified equally sized bins based on mean annual temperature outperformed models calibrated with all 500 sites (i.e. full sample) and led to lowest RMSE. This result is in line with the conclusions by Cochran (1946) and Bourdeau (1953) that random components are beneficial in ecological studies and stratified sampling represents a population equally or better than random sampling. Even more remarkable is that the calculation time of the calibrations for models trained with these stratified samples was notably shorter than for models trained with the full sample. Therefore, we recommend stratified sampling based on mean annual temperature for the calibration of species-specific models, since it leads to the best model performance at the population level while requiring very little computational resources.

Sample size effects suggested to calibrate with at least nine observations per free model parameter (N:q) to prevent serious overfitting. We estimated the degree of the bias-variance trade-off with the ratio between external and internal RMSE (Cawley and Talbot, 2010, Sect. 5.2.1). Our results showed that, while this ratio decreases constantly, the rate of decrease changes notably between N:q = ~9 to ~12. This range is in line with the sometimes mentioned rule of thumb of at least N:q = 10 in regression analysis. Besides and more specific, Jenkins and Quintana-Ascencio (2020) suggest the use of at least N:q = 8 in

https://doi.org/10.5194/egusphere-2022-1423
Preprint. Discussion started: 31 January 2023

regression analysis if the variance of predictands is low and at least N:q = 25 when it is high. Although we calibrated process-oriented models and not a regression, these minimum N:q are in line with our study and thus seem to apply, too. Moreover, while N:q = 9 appear to be the minimum, we suggest the use of larger N:q if the model is calibrated with observations derived from more than one site to account for an increased variance.

4.4 Projections of autumn phenology

Overall, the climate projection scenarios were the primary drivers of the projected shifts in autumn phenology, with the warmer scenario causing later autumn phenology than the cooler scenario, which is consistent with the currently observed main effect of warming and indicates that the models largely agree that warming extends the growing season. Having the largest influence in two out of three projection modes, climate projection scenarios explained between 46% and 64% of the variance in the 100-year shifts of autumn phenology. On average, the projected autumn phenology occurred 8–9 days later when projected with the warmer RCP 8.5 than with the cooler RCP 4.5 scenarios, which corresponds to the observed main effect of warming. Past climate warming was found to mainly delay autumn phenology (Ibáñez et al., 2010; Meier et al., 2021), but slight forward shifts or a distribution around a temporal change rate of zero have also been observed (Menzel et al., 2020; Piao et al., 2019). Such inconsistent past trends may be explained by an autumn phenology that depends more on the severity than the type of weather event, with, for example, moderate heat spells causing backward shifts but extreme heat spells and drought causing forward shifts (Xie et al., 2015). Since the number and severity of heat spells is related to sites (e.g. warmer lowland vs. colder highland sites; Bigler and Vitasse, 2021), such opposing effects of weather events may explain the large influence of sites on projected shifts in autumn phenology, discussed below. In addition, the length of the growing season is affected by shifts in spring and autumn phenology for deciduous trees. Our projections were based on a spring phenology that advanced by 20 days within 100 years. Subsequently, the projected growing season lengthened by 7–32 days (RCP 4.5) or by 16–40 days (RCP 8.5), even when autumn phenology shifted forward, as projected with some models and discussed further below. Therefore, our study supports a general lengthening of the growing season due to projected climate warming, as also suggested by Delpierre et al. (2009), Keenan and Richardson (2015), or Meier et al. (2021), in contrast to (but see Zani et al., 2020).

The divergent autumn phenology projections of the scenario RCP 4.5 and CMC 2 might be due to temperature and precipitation biases in this scenario. We based our autumn phenology projections on 26 different climate model chains of the EURO CORDEX dataset, each consisting of a global and regional climate model (GCM and RCM, respectively; Supplement S1: Table S5). While the patterns in the projections generally matched our expectations, the projected autumn phenology based on the scenario RCP 4.5 and CMC 2 behaved differently from those based on the other scenarios (Fig. 4). The EURO CORDEX is a state of the art GCM and RCM ensemble and widely accepted to contain high quality climate projection data despite some biases (Coppola et al., 2021; Vautard et al., 2021). The afore mentioned RCP 4.5 and CMC 2 stands for the RCM CNRM-ALADIN63 (ALADIN63; Nabat et al., 2020) driven by the GCM CNRM-CERFACS-CNRM-CM5 (CM5; Voldoire et al., 2013) under RCP 4.5 (version two of the run r1i1p1; Supplement S1: Table S5). This scenario is the only one based on the RCM ALADIN63 in this study, whereas five other scenarios were also based on the GCM CM5. ALADIN63 is the successor

https://doi.org/10.5194/egusphere-2022-1423
Preprint. Discussion started: 31 January 2023

of CNRM-ALADIN53 (ALADIN53; Colin et al., 2010), which emerged after ten years of development and is arguably different from the latter but still related to it (Nabat et al., 2020). The GCM-RCM chain CM5 - ALADIN53 had comparatively great difficulty in accurately modeling the interannual and seasonal variability of mean temperature, seasonal precipitation for summer (i.e., June, July, and August; JJA), and the seasonal variability of different drought indices in a comparison of the historical runs from the EURO-CORDEX ensemble with observational data for southern Italy (Peres et al., 2020). Another comparison resulted in relatively large errors in the minimum temperature during summer (JJA) for both ALADIN53 and ALADIN63 driven by CM5 as well as in the second largest deviation from the observed temperature trend for CM5 - ALADIN63 (i.e. more than twice the temperature increase during 1970–2005 as observed) based on historical runs of the EURO-CORDEX ensemble and weather observations for the Pannonian Basin in the southeast of Central Europe (Lazić et al., 2021). Since we treated all GCM-RCM used in this study the same (Supplement S1: Sect. 2), it may be that such biases in temperature variability and summer temperature are responsible for the deviating projections of autumn phenology when based on RCP 4.5 and CMC 2.

Sites generally exhibited the second largest influence on projected shifts and had more influence when the latter were projected with species- than with site-specific models, which could be due to correct modelling of site differences, but poorer calibration for sites with phenology deviating from the sample mean seems more probable. Studies of past changes in autumn phenology of trees found ambiguous trends between different sites (Piao et al., 2019; Meier et al., 2021). Different trends may be the result of opposing weather effects, e.g. moderate versus severe heat and drought spells (Xie et al., 2015), or of different correlations between spring and autumn phenology, dependent on nutrient availability and elevation (Fu et al., 2019; Charlet De Sauvage et al., 2022). Thus, it may be that such opposing weather effects or different correlations led to the strong influence of sites on projected autumn phenology. However, this strong influence could also be due to the above-described tendency of models to the mean and subsequent poorer calibration for sites at the extremes of the climatic and phenological spectrum within samples. This hypothesis is further supported by the larger relative influence of sites on projections with species- than with site-specific models. In addition, species-specific models performed worse than site-specific models (based on converged runs without NA values), as was also reported by Basler (2016) with respect to models of spring phenology, while Liu et al. (2020) found that species-specific models poorly reflected the spatial variability of autumn phenology. Thus, it seems improbable that the species-specific models with generally poorer performance predicted site differences more accurately than the site-specific models with generally better performance. Therefore, we suspect that the large influence of sites on projections with species-specific models is primarily due to insufficiently modelled processes of leaf phenology and the consequent tendency of phenology models to the mean.

The influence of phenology models on projected autumn phenology was relatively low and the range of projections relatively small, which suggests that the analyzed models are generally based on the same process. The largest influence of phenology models was 11% and occurred in projections based on site-specific models and hence was almost six times smaller than the influence of climate projection scenarios. While the underlying processes differ between each model (Delpierre et al., 2009; Keenan and Richardson, 2015; Lang et al., 2019; Liu et al., 2019; Zani et al., 2020), the influence of these differences on the

https://doi.org/10.5194/egusphere-2022-1423
Preprint. Discussion started: 31 January 2023

projected autumn phenology did not affect the projected lengthening of the growing season: Different models altered the reference shifts by -12 to +2 days, which may result in forward shifts in autumn phenology with the cooler RCP 4.5 scenarios, but never in a shortening of the growing season because the latter is calculated in combination with the -20 days shift in spring phenology. Moreover, the difference between the models lay within 14 days (i.e. -12 to +2 days), which is less than the uncertainty attached to recordings of autumn phenology based on human observations (i.e. due to small sample sizes and observer bias; Liu et al., 2021). In other words, the different process-oriented models led to differences in the length of the growing season that were smaller than the uncertainty in the data upon which we based our projections. Therefore, our results justify the assumption, that the examined phenology models do not differ fundamentally in their underlying processes, even if we acknowledge that the TDM, PDM, and TPDM models (Liu et al., 2019) behaved differently than the other models (i.e. they resulted in the largest forward or smallest backward shifts of autumn phenology). Rather, we suggest that all analyzed models are based on the same process but simplify it in different ways.

Better-performing models generally projected a lengthening of the growing season, which may add a new dimension to the discussion about realistic projections of autumn leaf phenology, but should be treated with caution, as corresponding correlations were relatively low. The PIA models in Zani et al. (2020) projected autumn phenology to advance and caused a shortening of the growing season between the years 2000 and 2100 as a result of increased photosynthetic activity. This result has thus been debated (Norby, 2021; Zani et al., 2021; Lu and Keenan, 2022) and could not be reproduced in our study. Here, we found positive and negative coefficient estimates, depending on the projection mode, which seems to be partly in line with Zani et al. (2020), but that is actually not the case: First, our estimates refer to changes relative to the reference, which was always positive. Thus, while the negative coefficients for the PIA models indicated negative deviations from the reference, they still resulted in later autumn phenology and longer growing seasons. Second, Zani et al. (2020) reported an advancement of autumn phenology only for projections based on PIA models and in contrast to the other models, while our results suggest the largest forward shifts for the TDM, PDM, and TPDM models (Liu et al., 2019). Moreover, the negative correlations between phenology models ranked by their performance and projection estimates showed that models with smaller root mean square errors generally projected larger shifts than models with larger root mean square errors. In other words, while we were unable to replicate the projected pronounced forward shifts in autumn phenology due to increased photosynthetic activity, our results suggest that better performing models tend to project a later autumn phenology.

4.5 Methodological issues

4.5.1 Treatment of NA values and non-converging calibration runs

Especially the ranks of site-specific phenology models and corresponding optimization algorithms were affected by the treatment of NA values and non-convergent calibration runs. Here, we performed two analyses in which we either replaced NA values and non-convergent runs with a fixed value or we excluded the affected runs. We are not aware of any other study involving process-oriented models of tree leaf phenology that has mentioned NA-producing or non-converging calibration

https://doi.org/10.5194/egusphere-2022-1423
Preprint. Discussion started: 31 January 2023

runs and their treatment. We doubt that our study is an exception in that it produced NAs or non-converging runs at all. Be that as it may, in the absence of previous studies addressing this issue, we could not refer to any established treatment and had to find a way to deal with NA values and non-converging runs. We chose (1) to penalize NAs with a replacement slightly larger than the largest modelled differences or (2) to exclude concerned runs. Since only "bad" runs were excluded, exclusion may bias the analysis by leading to overly optimistic results and replacement seemed preferrable, especially for ranking factors by their effect on performance. However, replacement adds an artificial effect and thus affects the estimated effect sizes, why they should be compared with corresponding effect sizes after exclusion and treated with caution. The models with the most parameters also led to the most NA-producing or non-converging runs, especially with site-specific calibration performed with GenSA or Bayesian optimization algorithms. Subsequently, we found considerable differences between the ranking of phenology models and optimization algorithms depending on the treatments with replacement and exclusion.

4.5.2 Evaluation of model performance based on the root mean square error

We evaluated model performance solely based on the RMSE, which allows only limited conclusions to be drawn about biological processes but reveals the effects of various factors on model performance and projections. Small RMSE values may also result from poorly calibrated models, due to intercorrelation between free model parameters or limited data (e.g. regarding the base temperature and threshold in the CDD model or climatic and temporal sections of the habitat and life span of a species, respectively; Chuine and Régnière, 2017). Therefore, Chuine and Régnière (2017) recommended to complement the quantitative evaluation with a qualitative assessment of the calibrated parameters and the resulting curves of the rate functions. Since we were less interested in the biological processes that drive leaf phenology and since we evaluated over 2 million different models, we refrained from a qualitative assessment and focused solely on the quantitative RMSE. Therefore, conclusions about the processes driving autumn phenology should be drawn from our study with caution. At the same time, the RMSE remains an important measure for model comparison and selection. Thus, our conclusions about the relationships between the factors analyzed and model performance or projections, and between model performance and projections, are relevant for future studies of leaf phenology.

4.5.3 Choice of generalized additive models instead of linear mixed-effects models

We opted for generalized additive models rather than linear mixed-effects models due to software limitations and thus benefited from higher computing speed without affecting the results. The amount of Δ_{100} data was too large and thus the variance-covariance matrix could not be solved by the LAPACK library (Anderson et al., 1999) integrated in R (R Core Team, 2022) and called upon by the function lme4::lmer (Bates et al., 2015). However, the data could be processed with the function mgcv::bam (Wood, 2011, 2017), which allowed an alternative formulation of a linear model with random intercepts. While mgcv::bam was much faster than lme4::lmer (personal observation), the corresponding coefficient estimates were practically identical (comparison not shown).

https://doi.org/10.5194/egusphere-2022-1423
Preprint. Discussion started: 31 January 2023

4.5.4 Evaluation based on sampled model projections

Since we feared hardware limitations if we evaluated all Δ_{100} data, we opted for an evaluation based on samples, the results of which are convincing. While we were able to fit the generalized additive models for all Δ_{100} data, the subsequent analysis of variance (functions aov and drop1 in the R package stats; R Core Team, 2022) required an enormous amount of computing power (>600 GB RAM per CPU-core for the smallest dataset, i.e. the projections based on site-specific calibration). Therefore, we reduced the amount of data to be processed by drawing samples, fitting a generalized additive model for each sample, and deriving an ANOVA from each model. Since the resulting coefficient estimates, confidence intervals, and estimates of the relative explained variance were within reasonable ranges, this procedure further strengthened our confidence in our results.

4.5.5 Significance level and Bayes factors

We chose a lower significance level than commonly used in ecology studies and complemented the *p*-value with the minimum Bayes factor to prevent over- or misinterpretation of our results and found our data to strongly encourage further research. The *p*-values decrease as datasets and measurement precision increase (Wasserstein and Lazar, 2016), and the analysis of many coefficients increases the probability of type I errors (i.e. “false positives”; Oxman and Guyatt, 1992; Ioannidis, 2005). Further, the *p*-value is often misinterpreted (Goodman, 2008) and biased (Ioannidis, 2019), which may lead to overinterpretation of scientific results. We have accounted for these relations and possible overinterpretations by choosing a lower significance level than commonly used in ecology studies and complementing the *p*-value with the minimum Bayes factor of the null to the alternative hypothesis. While ecological studies generally apply a significance level of $\alpha = 0.05$, we applied a smaller level of $\alpha = 0.01$ and thus a threshold of $p = 0.005$ for two-sided distributions. Even with this lower α, most coefficients in our generalized additive model fits and ANOVAs were significant. Further, most of our statistically significant findings were accompanied by a minimum Bayes factor of 1/1000 or lower, indicating that our data suggest with decisive evidence that “no effect” (i.e. the null hypothesis) is unlikely. As our study was exploratory, we believe that further studies to verify or falsify and quantify the presumed effects are worthwhile and will provide exciting new insights.

5 Conclusion

Based on our combined results, we recommend (1) species-specific models for the analysis of underlying phenology processes and for projections, (2) a combination of samples for cross-validation and independent test samples, and (3) to consider a possible tendency to the mean underlying the models. The choice of species- rather than site-specific models leads to generally larger sample sizes and larger ranges of considered drivers. In addition, species-specific models facilitate the assessment of the extent to which calibrated models tend towards the mean observation due to insufficient consideration of relevant processes. We advocate cross-validation of possibly regional, species-specific models, followed by independent tests. Specifically, we propose that (1) sites are selected in a stratified procedure based on annual mean temperature for (2) the cross-validation of a species-specific model with systematically balanced observations selected based on site and year, before (3) the calibrated

https://doi.org/10.5194/egusphere-2022-1423
Preprint. Discussion started: 31 January 2023

model is tested with new sites selected in a stratified procedure based on phenology. For both cross-validation and testing, the degree to which the model tends to the mean should be examined to assess how well the models perform at individual sites, within the entire region of interest, and, where possible, under different climate regimes.

We conclude that generally uncertain projections tend towards a lengthening of the growing season. Accurate projections of changes in the length of the growing season under projected climate change are essential for our understanding of the future CO_2 mitigating capacity and of future species compositions and distributions of forests. Our results suggest that projected autumn leaf phenology will be delayed due to projected climate warming, and thus the projected length of the growing season will increase. However, this result appears to be based on models that respond to quite similar underlying processes and may underestimate adverse effects of climate warming on autumn phenology, such as severe droughts. Therefore, further studies are needed to develop models that adequately account for processes relevant to autumn leaf phenology, and thus provide more valid projections.

Code and data availability

All manuscript related raw data are publicly available, properly referenced, and listed in Supplement S1: Table S7. The modelled and projected autumn phenology data is openly accessible under https://doi.org/10.5061/dryad.dv41ns22k and https://doi.org/10.5061/dryad.mw6m90613, respectively. In addition, the manuscript related R code for the phenology models is openly accessible under https://doi.org/10.5281/zenodo.7188160.

Author contribution

This study was conceptualized by MM and CB. MM adapted the code of the process-oriented models and performed the simulations. MM analyzed the simulations with contributions from CB and visualized the results. The manuscript was prepared by MM with contributions from CB.

Competing interests

The authors declare that they have no conflict of interest.

Acknowledgements

We thank Deborah Zani and Constantin Zohner for the informative discussions about their study (Zani et al., 2020) and the applied code for the phenology models (Zanid90, 2021), which we adapted for our study. We further thank Lidong Mo and Constantin Zohner from the Crowther Lab at ETH Zurich to share their code to download climate data from the Google Earth Engine (Gorelick et al., 2017), which we adapted for our study. We also thank Hussain Abbas from the Forest Ecology group

https://doi.org/10.5194/egusphere-2022-1423
Preprint. Discussion started: 31 January 2023

of ETH Zurich for his helpful advice and support with the batch system and the management of the computational jobs. Calibrations and projections of the phenology models, fits of the generalized additive models and subsequent analyses of variance were performed on the Euler cluster operated by the High Performance Computing group at ETH Zurich. This study is part of the project "Assessing climate influences on tree phenology and growth rates" (PheGro-Clim) at ETH Zurich, which was funded by the Swiss National Science Foundation SNSF (SNSF project number 179144).

References

Anderson, E., Bai, Z., Bischof, C., Blackford, L. S., Demmel, J., Dongarra, J., Du Croz, J., Greenbaum, A., Hammarling, S., McKenney, A., and Sorensen, D.: LAPACK users' guide, Third, Society for Industrial and Applied Mathematics, SIAM, Philadelphia, PA1999.

Arend, M., Gessler, A., and Schaub, M.: The influence of the soil on spring and autumn phenology in European beech, Tree Physiol., 36, 78-85, 10.1093/treephys/tpv087, 2016.

Asse, D., Chuine, I., Vitasse, Y., Yoccoz, N. G., Delpierre, N., Badeau, V., Delestrade, A., and Randin, C. F.: Warmer winters reduce the advance of tree spring phenology induced by warmer springs in the Alps, Agricultural and Forest Meteorology, 252, 220-230, 10.1016/j.agrformet.2018.01.030, 2018.

Basler, D.: Evaluating phenological models for the prediction of leaf-out dates in six temperate tree species across central Europe, Agricultural and Forest Meteorology, 217, 10-21, 10.1016/j.agrformet.2015.11.007, 2016.

Bates, D., Machler, M., Bolker, B. M., and Walker, S. C.: Fitting Linear Mixed-Effects Models Using lme4, J. Stat. Softw., 67, 1-48, 2015.

Beaudoing, H. and Rodell, M.: GLDAS Noah Land Surface Model L4 3 hourly 0.25 x 0.25 degree V2.0, Goddard Earth Sciences Data and Information Services Center (GES DISC) [dataset], 10.5067/342OHQM9AK6Q, 2019.

Beaudoing, H. and Rodell, M.: GLDAS Noah Land Surface Model L4 3 hourly 0.25 x 0.25 degree V2.1, Goddard Earth Sciences Data and Information Services Center (GES DISC) [dataset], 10.5067/E7TYRXPJKWOQ, 2020.

Bendtsen, C.: pso: Particle Swarm Optimization. R package version 1.0.4, 2012.

Benjamin, D. J. and Berger, J. O.: Three Recommendations for Improving the Use of p-Values, The American Statistician, 73, 186-191, 10.1080/00031305.2018.1543135, 2019.

Bigler, C. and Vitasse, Y.: Premature leaf discoloration of European deciduous trees is caused by drought and heat in late spring and cold spells in early fall, Agricultural and Forest Meteorology, 307, 108492, https://doi.org/10.1016/j.agrformet.2021.108492, 2021.

Bourdeau, P. F.: A Test of Random Versus Systematic Ecological Samplig, Ecology, 34, 499-512, 10.2307/1929722, 1953.

Braconnot, P., Harrison, S. P., Kageyama, M., Bartlein, P. J., Masson-Delmotte, V., Abe-Ouchi, A., Otto-Bliesner, B., and Zhao, Y.: Evaluation of climate models using palaeoclimatic data, Nat. Clim. Chang., 2, 417-424, 10.1038/nclimate1456, 2012.

Brock, T. D.: Calculating solar radiation for ecological studies, Ecol. Model., 14, 1-19, 10.1016/0304-3800(81)90011-9, 1981.

Caffarra, A., Donnelly, A., and Chuine, I.: Modelling the timing of Betula pubescens budburst. II. Integrating complex effects of photoperiod into process-based models, Clim. Res., 46, 159-170, 10.3354/cr00983, 2011.

Cawley, G. C. and Talbot, N. L. C.: On Over-fitting in Model Selection and Subsequent Selection Bias in Performance Evaluation, J. Mach. Learn. Res., 11(70): 2079−2107, 2010.

Chandler, R. E. and Scott, E. M.: Statistical methods for trend detection and analysis in the environmental sciences, Statistics in practice, Wiley, Chichester, 368 S. pp.2011.

Charlet de Sauvage, J., Vitasse, Y., Meier, M., Delzon, S., and Bigler, C.: Temperature rather than individual growing period length determines radial growth of sessile oak in the Pyrenees, Agricultural and Forest Meteorology, 317, 108885, https://doi.org/10.1016/j.agrformet.2022.108885, 2022.

Chen, L., Huang, J. G., Ma, Q. Q., Hanninen, H., Rossi, S., Piao, S. L., and Bergeron, Y.: Spring phenology at different altitudes is becoming more uniform under global warming in Europe, Global Change Biology, 24, 3969-3975, 10.1111/gcb.14288, 2018.

Chuine, I.: Why does phenology drive species distribution?, Philos. Trans. R. Soc. B-Biol. Sci., 365, 3149-3160, 10.1098/rstb.2010.0142, 2010.

Chuine, I. and Beaubien, E. G.: Phenology is a major determinant of tree species range, Ecol. Lett., 4, 500-510, 10.1046/j.1461-0248.2001.00261.x, 2001.

Chuine, I. and Régnière, J.: Process-Based Models of Phenology for Plants and Animals, Annual Review of Ecology, Evolution, and Systematics, 48, 159-182, 10.1146/annurev-ecolsys-110316-022706, 2017.

Chuine, I., Cour, P., and Rousseau, D. D.: Fitting models predicting dates of flowering of temperate-zone trees using simulated annealing, Plant, Cell & Environment, 21, 455-466, 10.1046/j.1365-3040.1998.00299.x, 1998.

https://doi.org/10.5194/egusphere-2022-1423
Preprint. Discussion started: 31 January 2023

Chuine, I., Cour, P., and Rousseau, D. D.: Selecting models to predict the timing of flowering of temperate trees: implications for tree phenology modelling, Plant Cell Environ., 22, 1-13, 10.1046/j.1365-3040.1999.00395.x, 1999.

Chuine, I., de Cortazar-Atauri, I. G., Kramer, K., and Hänninen, H.: Plant Development Models, in: Phenology: An Integrative Environmental Science, edited by: Schwartz, M. D., Springer Netherlands, Dordrecht, 275-293, 10.1007/978-94-007-6925-0_15, 2013.

Clark, M.: mixedup: Miscellaneous functions for mixed models. R package version 0.3.9. https://m-clark.github.io/mixedup, 2022.

Clarke, L., Edmonds, J., Jacoby, H., Pitcher, H., Reilly, J., and Richels, R.: Scenarios of Greenhouse Gas Emissions and Atmospheric Concentrations. Sub-Report 2.1a of Synthesis and Assessment Product 2.1 by the U.S. Climate Change Science Program and the Subcommittee on Global Change Research, Department of Energy, Office of Biological & Environmental Research, Washington DC, 2007.

Clerc, M.: From Theory to Practice in Particle Swarm Optimization, in: Handbook of Swarm Intelligence: Concepts, Principles and Applications, edited by: Panigrahi, B. K., Shi, Y., and Lim, M.-H., Springer Berlin Heidelberg, Berlin, Heidelberg, 3-36, 10.1007/978-3-642-17390-5_1, 2011.

Clerc, M.: Standard Particle Swarm Optimisation. hal-00764996. https://hal.archives-ouvertes.fr/hal-00764996, 2012.

Colin, J., Déqué, M., Radu, R., and Somot, S.: Sensitivity study of heavy precipitation in Limited Area Model climate simulations: influence of the size of the domain and the use of the spectral nudging technique, Tellus A: Dynamic Meteorology and Oceanography, 62, 591-604, 10.1111/j.1600-0870.2010.00467.x, 2010.

Coppola, E., Nogherotto, R., Ciarlo', J. M., Giorgi, F., van Meijgaard, E., Kadygrov, N., Iles, C., Corre, L., Sandstad, M., Somot, S., Nabat, P., Vautard, R., Levavasseur, G., Schwingshackl, C., Sillmann, J., Kjellström, E., Nikulin, G., Aalbers, E., Lenderink, G., Christensen, O. B., Boberg, F., Sørland, S. L., Demory, M.-E., Bülow, K., Teichmann, C., Warrach-Sagi, K., and Wulfmeyer, V.: Assessment of the European Climate Projections as Simulated by the Large EURO-CORDEX Regional and Global Climate Model Ensemble, Journal of Geophysical Research: Atmospheres, 126, e2019JD032356, https://doi.org/10.1029/2019JD032356, 2021.

de Réaumur, R. A. F.: Observations du thermomètre, faites à Paris pendant l'année 1735, comparées avec celles qui ont été faites sous la ligne, à l'isle de France, a Alger et quelques-unes de nos isles de l'Amérique, Académie royale des sciences, des lettres et des beaux-arts de Belgique, 33, 1735.

Delpierre, N., Dufrene, E., Soudani, K., Ulrich, E., Cecchini, S., Boe, J., and Francois, C.: Modelling interannual and spatial variability of leaf senescence for three deciduous tree species in France, Agricultural and Forest Meteorology, 149, 938-948, 10.1016/j.agrformet.2008.11.014, 2009.

Dowle, M. and Srinivasan, A.: data.table: Extension of `data.frame`. R package version 1.14.2. https://CRAN.R-project.org/package=data.table, 2021.

Dufrêne, E., Davi, H., Francois, C., le Maire, G., Le Dantec, V., and Granier, A.: Modelling carbon and water cycles in a beech forest Part I: Model description and uncertainty analysis on modelled NEE, Ecol. Model., 185, 407-436, 10.1016/j.ecolmodel.2005.01.004, 2005.

Dupuy, D., Helbert, C., and Franco, J.: DiceDesign and DiceEval: Two R Packages for Design and Analysis of Computer Experiments, J. Stat. Softw., 65, 1 - 38, 10.18637/jss.v065.i11, 2015.

Foley, A. M.: Uncertainty in regional climate modelling: A review, Progress in Physical Geography: Earth and Environment, 34, 647-670, 10.1177/0309133310375654, 2010.

Fu, Y., Li, X., Zhou, X., Geng, X., Guo, Y., and Zhang, Y.: Progress in plant phenology modeling under global climate change, Science China Earth Sciences, 63, 1237-1247, 10.1007/s11430-019-9622-2, 2020.

Fu, Y. H., Piao, S. L., Op de Beeck, M., Cong, N., Zhao, H. F., Zhang, Y., Menzel, A., and Janssens, I. A.: Recent spring phenology shifts in western Central Europe based on multiscale observations, Glob. Ecol. Biogeogr., 23, 1255-1263, 10.1111/geb.12210, 2014a.

Fu, Y. H., Piao, S. L., Delpierre, N., Hao, F. H., Hanninen, H., Geng, X. J., Penuelas, J., Zhang, X., Janssens, I. A., and Campioli, M.: Nutrient availability alters the correlation between spring leaf-out and autumn leaf senescence dates, Tree Physiol., 39, 1277-1284, 10.1093/treephys/tpz041, 2019.

Fu, Y. S. H., Campioli, M., Vitasse, Y., De Boeck, H. J., Van den Berge, J., AbdElgawad, H., Asard, H., Piao, S. L., Deckmyn, G., and Janssens, I. A.: Variation in leaf flushing date influences autumnal senescence and next year's flushing date in two temperate tree species, Proc. Natl. Acad. Sci. U. S. A., 111, 7355-7360, 10.1073/pnas.1321727111, 2014b.

Gill, A. L., Gallinat, A. S., Sanders-DeMott, R., Rigden, A. J., Gianotti, D. J. S., Mantooth, J. A., and Templer, P. H.: Changes in autumn senescence in northern hemisphere deciduous trees: a meta-analysis of autumn phenology studies, Ann. Bot., 116, 875-888, 10.1093/aob/mcv055, 2015.

Goodman, S.: A Dirty Dozen: Twelve P-Value Misconceptions, Seminars in Hematology, 45, 135-140, https://doi.org/10.1053/j.seminhematol.2008.04.003, 2008.

Gorelick, N., Hancher, M., Dixon, M., Ilyushchenko, S., Thau, D., and Moore, R.: Google Earth Engine: Planetary-scale geospatial analysis for everyone, Remote Sens. Environ., 202, 18-27, 10.1016/j.rse.2017.06.031, 2017.

Hack, H., Bleiholder, H., Buhr, L., Meier, U., Schnock-Fricke, U., Weber, E., and Witzenberger, A.: Einheitliche codierung der phänologischen entwicklungsstadien mono-und dikotyler pflanzen–erweiterte BBCH-Skala, Allgemein, Nachrichtenbl. Deut. Pflanzenschutzd, 44, 265-270, 1992.

https://doi.org/10.5194/egusphere-2022-1423
Preprint. Discussion started: 31 January 2023

Hansen, N.: The CMA Evolution Strategy: A Comparing Review, in: Towards a New Evolutionary Computation: Advances in the Estimation of Distribution Algorithms, edited by: Lozano, J. A., Larrañaga, P., Inza, I., and Bengoetxea, E., Springer Berlin Heidelberg, Berlin, Heidelberg, 75-102, 10.1007/3-540-32494-1_4, 2006.
Hansen, N.: The CMA evolution strategy: A tutorial, arXiv preprint arXiv:1604.00772, 2016.
Held, L. and Ott, M.: How the Maximal Evidence of P-Values Against Point Null Hypotheses Depends on Sample Size, The American Statistician, 70, 335-341, 10.1080/00031305.2016.1209128, 2016.
Held, L. and Ott, M.: On p-Values and Bayes Factors, Annual Review of Statistics and Its Application, 5, 393-419, 10.1146/annurev-statistics-031017-100307, 2018.
Hengl, T., Mendes de Jesus, J., Heuvelink, G. B. M., Ruiperez Gonzalez, M., Kilibarda, M., Blagotić, A., Shangguan, W., Wright, M. N., Geng, X., Bauer-Marschallinger, B., Guevara, M. A., Vargas, R., MacMillan, R. A., Batjes, N. H., Leenaars, J. G. B., Ribeiro, E., Wheeler, I., Mantel, S., and Kempen, B.: SoilGrids250m: Global gridded soil information based on machine learning, PLOS ONE, 12, e0169748, 10.1371/journal.pone.0169748, 2017.
Herr, D. G.: On the History of ANOVA in Unbalanced, Factorial Designs: The First 30 Years, The American Statistician, 40, 265-270, 10.2307/2684597, 1986.
Hufkens, K., Basler, D., Milliman, T., Melaas, E. K., and Richardson, A. D.: An integrated phenology modelling framework in R, Methods Ecol. Evol., 9, 1276-1285, 10.1111/2041-210x.12970, 2018.
Ibáñez, I., Primack, R. B., Miller-Rushing, A. J., Ellwood, E., Higuchi, H., Lee, S. D., Kobori, H., and Silander, J. A.: Forecasting phenology under global warming, Philos. Trans. R. Soc. B-Biol. Sci., 365, 3247-3260, 10.1098/rstb.2010.0120, 2010.
Ioannidis, J. P. A.: Why Most Published Research Findings Are False, PLOS Medicine, 2, e124, 10.1371/journal.pmed.0020124, 2005.
Ioannidis, J. P. A.: What Have We (Not) Learnt from Millions of Scientific Papers with P Values?, Am. Stat., 73, 20-25, 10.1080/00031305.2018.1447512, 2019.
Jacob, D., Petersen, J., Eggert, B., Alias, A., Christensen, O. B., Bouwer, L. M., Braun, A., Colette, A., Deque, M., Georgievski, G., Georgopoulou, E., Gobiet, A., Menut, L., Nikulin, G., Haensler, A., Hempelmann, N., Jones, C., Keuler, K., Kovats, S., Kroner, N., Kotlarski, S., Kriegsmann, A., Martin, E., van Meijgaard, E., Moseley, C., Pfeifer, S., Preuschmann, S., Radermacher, C., Radtke, K., Rechid, D., Rounsevell, M., Samuelsson, P., Somot, S., Soussana, J. F., Teichmann, C., Valentini, R., Vautard, R., Weber, B., and Yiou, P.: EURO-CORDEX: new high-resolution climate change projections for European impact research, Reg. Envir. Chang., 14, 563-578, 10.1007/s10113-013-0499-2, 2014.
James, G., Witten, D., Hastie, T., and Tibishirani, R.: An Introduction to Statistical Learning: with Applications in R, Springer, New York a.o., DOI 10.1007/978-1-4614-7138-7, 2017.
Jenkins, D. G. and Quintana-Ascencio, P. F.: A solution to minimum sample size for regressions, PLOS ONE, 15, e0229345, 10.1371/journal.pone.0229345, 2020.
Johnson, V. E.: Bayes Factors Based on Test Statistics, Journal of the Royal Statistical Society. Series B (Statistical Methodology), 67, 689-701, 2005.
Kassambara, A.: ggpubr: 'ggplot2' Based Publication Ready Plots. R package version 0.4.0. https://CRAN.R-project.org/package=ggpubr, 2020.
Keenan, R. J.: Climate change impacts and adaptation in forest management: a review, Ann. For. Sci., 72, 145-167, 10.1007/s13595-014-0446-5, 2015.
Keenan, T. F. and Richardson, A. D.: The timing of autumn senescence is affected by the timing of spring phenology: implications for predictive models, Glob Chang Biol, 21, 2634-2641, 10.1111/gcb.12890, 2015.
Keenan, T. F., Gray, J., Friedl, M. A., Toomey, M., Bohrer, G., Hollinger, D. Y., Munger, J. W., O'Keefe, J., Schmid, H. P., Wing, I. S., Yang, B., and Richardson, A. D.: Net carbon uptake has increased through warming-induced changes in temperate forest phenology, Nat. Clim. Chang., 4, 598-604, 10.1038/nclimate2253, 2014.
Kendall, M. G.: A new measure of rank correlation, Biometrika, 30, 81-93, 10.1093/biomet/30.1-2.81, 1938.
Krige, D.: A statistical approach to some mine valuations and allied problems at the Witwatersrand, Unpublished Master's Thesis, University of the Witwatersrand, Witwatersrand, South Africa, 1951.
Lang, G. A., Early, J. D., Martin, G. C., and Darnell, R. L.: Endo-, para-, and ecodormancy: Physiological teriminology and classification for dormancy research, Hortscience, 22, 371-377, 1987.
Lang, W., Chen, X., Qian, S., Liu, G., and Piao, S.: A new process-based model for predicting autumn phenology: How is leaf senescence controlled by photoperiod and temperature coupling?, Agricultural and Forest Meteorology, 268, 124-135, 10.1016/j.agrformet.2019.01.006, 2019.
Lazić, I., Tošić, M., and Djurdjević, V.: Verification of the EURO-CORDEX RCM Historical Run Results over the Pannonian Basin for the Summer Season, Atmosphere, 12, 714, 2021.
Liang, L. and Wu, J. X.: An empirical method to account for climatic adaptation in plant phenology models, Int. J. Biometeorol., 65, 1953-1966, 10.1007/s00484-021-02152-7, 2021.
Lieth, H.: Purposes of a Phenology Book, in: Phenology and Seasonality Modeling, edited by: Lieth, H., Springer Berlin Heidelberg, Berlin, Heidelberg, 3-19, 10.1007/978-3-642-51863-8_1, 1974.

https://doi.org/10.5194/egusphere-2022-1423
Preprint. Discussion started: 31 January 2023

Liu, G., Chen, X. Q., Fu, Y. S., and Delpierre, N.: Modelling leaf coloration dates over temperate China by considering effects of leafy season climate, Ecol. Model., 394, 34-43, 10.1016/j.ecolmodel.2018.12.020, 2019.
Liu, G., Chuine, I., Denechere, R., Jean, F., Dufrene, E., Vincent, G., Berveiller, D., and Delpierre, N.: Higher sample sizes and observer inter-calibration are needed for reliable scoring of leaf phenology in trees, Journal of Ecology, 14, 10.1111/1365-2745.13656, 2021.
Liu, Q., Piao, S. L., Campioli, M., Gao, M. D., Fu, Y. S. H., Wang, K., He, Y., Li, X. Y., and Janssens, I. A.: Modeling leaf senescence of deciduous tree species in Europe, Global Change Biology, 15, 10.1111/gcb.15132, 2020.
Lu, X. and Keenan, T. F.: No evidence for a negative effect of growing season photosynthesis on leaf senescence timing, Global Change Biology, n/a, https://doi.org/10.1111/gcb.16104, 2022.
Mao, J. and Yan, B.: Global Monthly Mean Leaf Area Index Climatology, 1981-2015 [dataset], https://doi.org/10.3334/ORNLDAAC/1653, 2019.
Marini, F. and Walczak, B.: Particle swarm optimization (PSO). A tutorial, Chemometrics and Intelligent Laboratory Systems, 149, 153-165, https://doi.org/10.1016/j.chemolab.2015.08.020, 2015.
Maurya, J. P. and Bhalerao, R. P.: Photoperiod- and temperature-mediated control of growth cessation and dormancy in trees: a molecular perspective, Ann. Bot., 120, 351-360, 10.1093/aob/mcx061, 2017.
Meier, M.: Process-oriented models of autumn leaf phenology (1.0). Zenodo. https://doi.org/10.5281/zenodo.7188160, 10.5281/zenodo.7188160, 2022.
Meier, M., Fuhrer, J., and Holzkamper, A.: Changing risk of spring frost damage in grapevines due to climate change? A case study in the Swiss Rhone Valley, Int. J. Biometeorol., 62, 991-1002, 10.1007/s00484-018-1501-y, 2018.
Meier, M., Vitasse, Y., Bugmann, H., and Bigler, C.: Phenological shifts induced by climate change amplify drought for broad-leaved trees at low elevations in Switzerland, Agricultural and Forest Meteorology, 307, 108485, https://doi.org/10.1016/j.agrformet.2021.108485, 2021.
Meier, U.: Growth stages of mono-and dicotyledonous plants, 2. Edition, Blackwell Wissenschafts-Verlag, 157 pp.2001.
Meinshausen, M., Smith, S. J., Calvin, K., Daniel, J. S., Kainuma, M. L. T., Lamarque, J. F., Matsumoto, K., Montzka, S. A., Raper, S. C. B., Riahi, K., Thomson, A., Velders, G. J. M., and van Vuuren, D. P. P.: The RCP greenhouse gas concentrations and their extensions from 1765 to 2300, Climatic Change, 109, 213-241, 10.1007/s10584-011-0156-z, 2011.
Meinshausen, M., Vogel, E., Nauels, A., Lorbacher, K., Meinshausen, N., Etheridge, D. M., Fraser, P. J., Montzka, S. A., Rayner, P. J., Trudinger, C. M., Krummel, P. B., Beyerle, U., Canadell, J. G., Daniel, J. S., Enting, I. G., Law, R. M., Lunder, C. R., O'Doherty, S., Prinn, R. G., Reimann, S., Rubino, M., Velders, G. J. M., Vollmer, M. K., Wang, R. H. J., and Weiss, R.: Historical greenhouse gas concentrations for climate modelling (CMIP6), Geosci. Model Dev., 10, 2057-2116, 10.5194/gmd-10-2057-2017, 2017.
Menzel, A., Yuan, Y., Matiu, M., Sparks, T., Scheifinger, H., Gehrig, R., and Estrella, N.: Climate change fingerprints in recent European plant phenology, Global Change Biology, 26, 14, 10.1111/gcb.15000, 2020.
Morin, X., Lechowicz, M. J., Augspurger, C., O' Keefe, J., Viner, D., and Chuine, I.: Leaf phenology in 22 North American tree species during the 21st century, Global Change Biology, 15, 961-975, 10.1111/j.1365-2486.2008.01735.x, 2009.
Nabat, P., Somot, S., Cassou, C., Mallet, M., Michou, M., Bouniol, D., Decharme, B., Drugé, T., Roehrig, R., and Saint-Martin, D.: Modulation of radiative aerosols effects by atmospheric circulation over the Euro-Mediterranean region, Atmos. Chem. Phys., 20, 8315-8349, 10.5194/acp-20-8315-2020, 2020.
Norby, R. J.: Comment on “Increased growing-season productivity drives earlier autumn leaf senescence in temperate trees”, Science, 371, eabg1438, 10.1126/science.abg1438, 2021.
Nuzzo, R. L.: The Inverse Fallacy and Interpreting P Values, PM&R, 7, 311-314, https://doi.org/10.1016/j.pmrj.2015.02.011, 2015.
Oxman, A. D. and Guyatt, G. H.: A Consumer's Guide to Subgroup Analyses, Annals of Internal Medicine, 116, 78-84, 10.7326/0003-4819-116-1-78, 1992.
Palmer, T. N., Shutts, G. J., Hagedorn, R., Doblas-Reyes, F. J., Jung, T., and Leutbecher, M.: Representing model uncertainty in weather and climate prediction, Annual Review of Earth and Planetary Sciences, 33, 163-193, 10.1146/annurev.earth.33.092203.122552, 2005.
Peaucelle, M., Janssens, I., Stocker, B., Ferrando, A., Fu, Y., Molowny-Horas, R., Ciais, P., and Peñuelas, J.: Spatial variance of spring phenology in temperate deciduous forests is constrained by background climatic conditions, Nature Communications, 10, 10.1038/s41467-019-13365-1, 2019.
Peres, D. J., Senatore, A., Nanni, P., Cancelliere, A., Mendicino, G., and Bonaccorso, B.: Evaluation of EURO-CORDEX (Coordinated Regional Climate Downscaling Experiment for the Euro-Mediterranean area) historical simulations by high-quality observational datasets in southern Italy: insights on drought assessment, Nat. Hazards Earth Syst. Sci., 20, 3057-3082, 10.5194/nhess-20-3057-2020, 2020.
Piao, S. L., Liu, Q., Chen, A. P., Janssens, I. A., Fu, Y. S., Dai, J. H., Liu, L. L., Lian, X., Shen, M. G., and Zhu, X. L.: Plant phenology and global climate change: Current progresses and challenges, Global Change Biology, 25, 1922-1940, 10.1111/gcb.14619, 2019.
Picheny, V. and Ginsbourger, D.: Noisy kriging-based optimization methods: A unified implementation within the DiceOptim package, Computational Statistics & Data Analysis, 71, 1035-1053, 10.1016/j.csda.2013.03.018, 2014.
Picheny, V., Ginsbourger Green, D., and Roustant, O.: DiceOptim: Kriging-Based Optimization for Computer Experiments. R package version 2.1.1. https://CRAN.R-project.org/package=DiceOptim, 2021.
Pinheiro, J. C. and Bates, D. M.: Mixed-effects models in S and S-PLUS, Statistics and computing, Springer, New York, 528 S. pp.2000.
R Core Team: R: A language and environment for statistical computing. R Foundation for Statistical Computing, 2022.

https://doi.org/10.5194/egusphere-2022-1423
Preprint. Discussion started: 31 January 2023

Riahi, K., Grübler, A., and Nakicenovic, N.: Scenarios of long-term socio-economic and environmental development under climate stabilization, Technological Forecasting and Social Change, 74, 887-935, https://doi.org/10.1016/j.techfore.2006.05.026, 2007.
Riahi, K., Rao, S., Krey, V., Cho, C., Chirkov, V., Fischer, G., Kindermann, G., Nakicenovic, N., and Rafaj, P.: RCP 8.5—A scenario of comparatively high greenhouse gas emissions, Climatic Change, 109, 33, 10.1007/s10584-011-0149-y, 2011.
Richardson, A. D., Keenan, T. F., Migliavacca, M., Ryu, Y., Sonnentag, O., and Toomey, M.: Climate change, phenology, and phenological control of vegetation feedbacks to the climate system, Agricultural and Forest Meteorology, 169, 156-173, 10.1016/j.agrformet.2012.09.012, 2013.
Rodell, M., Houser, P. R., Jambor, U., Gottschalck, J., Mitchell, K., Meng, C. J., Arsenault, K., Cosgrove, B., Radakovich, J., Bosilovich, M., Entin, J. K., Walker, J. P., Lohmann, D., and Toll, D.: The global land data assimilation system, Bull. Amer. Meteorol. Soc., 85, 381-394, 10.1175/bams-85-3-381, 2004.
Smith, S. J. and Wigley, T. M. L.: Multi-gas forcing stabilization with Minicam, The Energy Journal, 2006.
Taherdoost, H.: Sampling Methods in Research Methodology; How to Choose a Sampling Technique for Research (April 10, 2016), International Journal of Academic Research in Management, Vol. 5, No. 2, 2016, 18-27, 2016.
Templ, B., Koch, E., Bolmgren, K., Ungersbock, M., Paul, A., Scheifinger, H., Rutishauser, T., Busto, M., Chmielewski, F. M., Hajkova, L., Hodzic, S., Kaspar, F., Pietragalla, B., Romero-Fresneda, R., Tolvanen, A., Vucetic, V., Zimmermann, K., and Zust, A.: Pan European Phenological database (PEP725): a single point of access for European data, Int J Biometeorol, 62, 1109-1113, 10.1007/s00484-018-1512-8, 2018.
Thomson, A. M., Calvin, K. V., Smith, S. J., Kyle, G. P., Volke, A., Patel, P., Delgado-Arias, S., Bond-Lamberty, B., Wise, M. A., Clarke, L. E., and Edmonds, J. A.: RCP4.5: a pathway for stabilization of radiative forcing by 2100, Climatic Change, 109, 77, 10.1007/s10584-011-0151-4, 2011.
Thoning, K. W., Crotwell, A. M., and Mund, J. W.: Atmospheric Carbon Dioxide Dry Air Mole Fractions from continuous measurements at Mauna Loa, Hawaii, Barrow, Alaska, American Samoa and South Pole. 1973-2020, Version 2021-08-09 [dataset], https://doi.org/10.15138/yaf1-bk21, 2021.
Trautmann, H., Mersmann, O., and Arnu , D.: cmaes: Covariance Matrix Adapting Evolutionary Strategy. R package version 1.0-12, 2011.
Vautard, R., Kadygrov, N., Iles, C., Boberg, F., Buonomo, E., Bülow, K., Coppola, E., Corre, L., van Meijgaard, E., Nogherotto, R., Sandstad, M., Schwingshackl, C., Somot, S., Aalbers, E., Christensen, O. B., Ciarlo, J. M., Demory, M.-E., Giorgi, F., Jacob, D., Jones, R. G., Keuler, K., Kjellström, E., Lenderink, G., Levavasseur, G., Nikulin, G., Sillmann, J., Solidoro, C., Sørland, S. L., Steger, C., Teichmann, C., Warrach-Sagi, K., and Wulfmeyer, V.: Evaluation of the Large EURO-CORDEX Regional Climate Model Ensemble, Journal of Geophysical Research: Atmospheres, 126, e2019JD032344, https://doi.org/10.1029/2019JD032344, 2021.
Vitasse, Y., Baumgarten, F., Zohner, C. M., Kaewthongrach, R., Fu, Y. H., Walde, M., and Moser, B.: Impact of microclimatic conditions and resource availability on spring and autumn phenology of temperate tree seedlings, New Phytol., 10.1111/nph.17606, 2021.
Voeten, C. C.: buildmer: Stepwise Elimination and Term Reordering for Mixed-Effects Regression. R package version 2.4, 2022.
Voldoire, A., Sanchez-Gomez, E., Salas y Mélia, D., Decharme, B., Cassou, C., Sénési, S., Valcke, S., Beau, I., Alias, A., Chevallier, M., Déqué, M., Deshayes, J., Douville, H., Fernandez, E., Madec, G., Maisonnave, E., Moine, M. P., Planton, S., Saint-Martin, D., Szopa, S., Tyteca, S., Alkama, R., Belamari, S., Braun, A., Coquart, L., and Chauvin, F.: The CNRM-CM5.1 global climate model: description and basic evaluation, Clim. Dyn., 40, 2091-2121, 10.1007/s00382-011-1259-y, 2013.
Wasserstein, R. L. and Lazar, N. A.: The ASA Statement on p-Values: Context, Process, and Purpose, The American Statistician, 70, 129-133, 10.1080/00031305.2016.1154108, 2016.
Wasserstein, R. L., Schirm, A. L., and Lazar, N. A.: Moving to a World Beyond "p < 0.05", Am. Stat., 73, 1-19, 10.1080/00031305.2019.1583913, 2019.
Wickham, H.: ggplot2: Elegant Graphics for Data Analysis, Springer-Verlag, New York2016.
Wickham, H. and Pedersen, T. L.: gtable: Arrange 'Grobs' in Tables. R package version 0.3.0. https://CRAN.R-project.org/package=gtable (R package version 0.3.0) [code], 2019.
Wise, M., Calvin, K., Thomson, A., Clarke, L., Bond-Lamberty, B., Sands, R., Smith, S. J., Janetos, A., and Edmonds, J.: Implications of Limiting CO2 Concentrations for Land Use and Energy, Science, 324, 1183-1186, doi:10.1126/science.1168475, 2009.
Wood, S. N.: Fast stable restricted maximum likelihood and marginal likelihood estimation of semiparametric generalized linear models, Journal of the Royal Statistical Society: Series B (Statistical Methodology), 73, 3-36, https://doi.org/10.1111/j.1467-9868.2010.00749.x, 2011.
Wood, S. N.: Generalized Additive Models: An Introduction with R, 2nd edition, Chapman and Hall/CRC, New York, https://doi.org/10.1201/9781315370279, 2017.
Xiang, Y., Sun, D. Y., Fan, W., and Gong, X. G.: Generalized simulated annealing algorithm and its application to the Thomson model, Phys. Lett. A, 233, 216-220, 10.1016/s0375-9601(97)00474-x, 1997.
Xiang, Y., Gubian, S., Martin, F., Suomela, B., and Hoeng, J.: Generalized Simulated Annealing for Global Optimization: The GenSA Package, R Journal, 5, 13-28, 10.32614/RJ-2013-002, 2013.
Xie, Y., Wang, X. J., and Silander, J. A.: Deciduous forest responses to temperature, precipitation, and drought imply complex climate change impacts, Proc. Natl. Acad. Sci. U. S. A., 112, 13585-13590, 10.1073/pnas.1509991112, 2015.

https://doi.org/10.5194/egusphere-2022-1423
Preprint. Discussion started: 31 January 2023

Xie, Y., Wang, X. J., Wilson, A. M., and Silander, J. A.: Predicting autumn phenology: How deciduous tree species respond to weather stressors, Agricultural and Forest Meteorology, 250, 127-137, 10.1016/j.agrformet.2017.12.259, 2018.

Xie, Z., Zhu, W. Q., Qiao, K., Li, P. X., and Liu, H.: Joint Influence Mechanism of Phenology and Climate on the Dynamics of Gross Primary Productivity: Insights From Temperate Deciduous Broadleaf Forests in North America, J. Geophys. Res.-Biogeosci., 126, 12, 10.1029/2020jg006049, 2021.

Yates, F.: The Analysis of Multiple Classifications with Unequal Numbers in the Different Classes, J. Am. Stat. Assoc., 29, 51-66, 10.2307/2278459, 1934.

Zambrano-Bigiarini, M.: hydroGOF: Goodness-of-fit functions for comparison of simulated and observed hydrological time series. https://github.com/hzambran/hydroGOF, DOI:10.5281/zenodo.839854., 2020.

Zani, D., Crowther, T. W., Mo, L., Renner, S. S., and Zohner, C. M.: Increased growing-season productivity drives earlier autumn leaf senescence in temperate trees, Science, 370, 1066-1071, 10.1126/science.abd8911, 2020.

Zani, D., Crowther, T. W., Mo, L., Renner, S. S., and Zohner, C. M.: Response to Comment on "Increased growing-season productivity drives earlier autumn leaf senescence in temperate trees", Science, 371, eabg2679, 10.1126/science.abg2679, 2021.

zanid90: zanid90/AutumnPhenology: Autumn Phenology repository [dataset], 10.5281/zenodo.4058162, 2021.

Zhao, H. F., Fu, Y. H., Wang, X. H., Zhang, Y., Liu, Y. W., and Janssens, I. A.: Diverging models introduce large uncertainty in future climate warming impact on spring phenology of temperate deciduous trees, Sci. Total Environ., 757, 10, 10.1016/j.scitotenv.2020.143903, 2021.

Zhu, Z. C., Bi, J., Pan, Y. Z., Ganguly, S., Anav, A., Xu, L., Samanta, A., Piao, S. L., Nemani, R. R., and Myneni, R. B.: Global Data Sets of Vegetation Leaf Area Index (LAI)3g and Fraction of Photosynthetically Active Radiation (FPAR)3g Derived from Global Inventory Modeling and Mapping Studies (GIMMS) Normalized Difference Vegetation Index (NDVI3g) for the Period 1981 to 2011, Remote Sens., 5, 927-948, 10.3390/rs5020927, 2013.